Nitration of Drp1 Provokes Mitophagy Activation Mediating Neuronal Injury in Experimental Autoimmune Encephalomyelitis

Wenting Li[1], Jinghan Feng[1], Chong Gao[1], Meiling Wu[1], Qiaohui Du[1], Bun Tsoi[1], Qi Wang[3], Dan Yang[2], Jiangang Shen[1, 3]*

Affiliations

1. School of Chinese Medicine, LKS Faculty of Medicine, The University of Hong Kong, Hong Kong SAR, China
2. Department of Chemistry, The University of Hong Kong, Hong Kong SAR, China
3. Institution of Clinical Pharmacology, Guangzhou University of Chinese Medicine, Guangzhou, China

Wenting Li (Email: lwenting@hku.hk), Jinghan Feng (Email: phyllisjinghan@163.com), Chong Gao (Email: chanderg@hotmail.com), Meiling Wu (Email: wumeilingcrow@hotmail.com), Qiaohui Du (Email: elvisdu@hku.hk), Bun Tsoi (Email: amytsoi@hku.hk), Qi Wang (E-mail: wangqi@gzucm.edu.cn), Dan Yang (Email: yangdan@hku.hk), Jiangang Shen (Email: shenjg@hku.hk)

Address correspondence to: Jiangang Shen, School of Chinese Medicine, LKS Faculty of Medicine, The University of Hong Kong, 10 Sassoon Road, Pokfulam, Hong Kong, Hong Kong SAR, China, Phone: 00852-39176429; Fax: 852-2168 4259; Email: shenjg@hkucc.hku.hk

Abbreviations

Drp1, Dynamin-related protein 1; dpi., Days postimmunization; dSTORM, Direct Stochastic Optical Reconstruction Microscopy; DTT, Dithiothreitol; EAE, Experimental autoimmune encephalomyelitis; LFB, Luxol fast blue; Mdivi-1, Mitochondrial Division Inhibitor 1MS, Multiple sclerosis; NO, Nitric oxide; $O_2^{\bullet-}$, Superoxide anion; $ONOO^-$, Peroxynitrite; PDC, Peroxynitrite decomposition catalyst; PFA, paraformaldehyde; PVDF, Polyvinylidene difluoride; TEM, Transmission electron microscopy; TUNEL, Terminal deoxynucleotidyl transferase-mediated dUTP nick end labeling; 3-MA, 3-Methyladenine; 3-NT, 3-nitrotyrosine.

Abstract

Active autophagy/mitophagy could mediate neurodegeneration and motor disabilities in multiple sclerosis (MS). Mitochondrial recruitment of dynamin-related protein 1 (Drp1) is a crucial step to initiate mitophagy. Peroxynitrite ($ONOO^-$) could be a player in MS pathology but the mechanisms remain unknown. We used animal model of experimental autoimmune encephalomyelitis (EAE) and tested whether $ONOO^-$ mediates Drp1 assembly in mitochondria for mitophagy and aggravates MS pathology. We found that autophagy/mitophagy activation was coincidently increased with axonal damage, apoptosis and disease progression in active EAE mice, which were remarkably attenuated by mitochondrial division/mitophagy inhibitor Mdivi-1. Importantly, increased $ONOO^-$ production was companied with Drp1 mitochondrial recruitment, PINK1/Parkin-mediated mitophagy, axonal degeneration and neuronal cell death, which were reversed by peroxynitrite decomposition catalyst (PDC). Furthermore, $ONOO^-$ production induced Drp1 nitration, promoted Drp1 assembly and mitochondrial recruitment for mitophagy activation, contributing to the EAE pathology. Together, we conclude that $ONOO^-$ serves as a key mediator in Drp1 nitration modification and assembly for facilitating mitophagy activation. Targeting $ONOO^-$-mediated Drp1 assembly and mitochondrial recruitment could be an important therapeutic strategy for multiple sclerosis treatment.

Key words

Dynamin-related protein 1, Nitration, Mitophagy, Neuronal Damages, Multiple sclerosis.

1. Introduction

Multiple sclerosis (MS) is clinically characterized by massive inflammatory infiltration, demyelination and axonal degradation, subsequently resulting in the motor disabilities [1]. Experimental autoimmune encephalomyelitis (EAE) is a widely adopted animal model mimicking the key features of MS, including CNS-directed leukocyte infiltrations and inflammatory microenvironment induction, which destroy CNS structures and lead to progressive paralysis [2]. Although large efforts have been made, the molecular mechanisms of MS are still largely unknown.

Autophagy, a “self-eating” process, appears to have both neuroprotective and detrimental roles in MS/EAE pathology. Mitophagy, defined by autophagic removal of damaged/dysfunctional mitochondria, is an important type of autophagy. Basal autophagy/mitophagy maintains cellular homeostasis by removing damaged components whereas excessive level could be a pathological process [3-5]. The roles of autophagy/mitophagy in MS or EAE rely on the cell-types, inflammatory/autoimmune status and stages of the disease progress. For example, autophagy activation in inflammatory cells aggravates disease progression during EAE injury due to the increased encephalitic cell survival [6]. Elevated autophagy promoted T cells survival and proliferation in EAE mice and MS patients [7]. Autophagy deficiency in dendritic cells or neutrophils reduced EAE severity [8, 9]. Neurons are the inflammatory/ autoimmune target cells. Activated autophagy, especially for mitophagy, was observed in motor neurons in EAE [10-13]. However, the roles of neuronal autophagy/mitophagy in MS pathology remain unclear yet. It is desirable to explore whether neuronal autophagy/mitophagy contributes to the MS/EAE pathology and affects motor function.

Oxidative stress is intimately associated autophagy/mitophagy in MS pathogenesis. Free radicals, mainly derived from macrophage/microglia, could induce oxidative damage, increase mitochondrial membrane permeability and initiate autophagosome formation, triggering bulk autophagy in EAE pathology [14]. As a representative RNS, nitric oxide (NO) rapidly reacts with superoxide anion ($O_2^{\bullet-}$) to form peroxynitrite

($ONOO^-$). $ONOO^-$ mediates oxidative damage and mitochondria dysfunction, etc. Human adult CNS-derived oligodendrocytes and motor neurons are highly susceptible to $ONOO^-$-mediated injury [15]. As an $ONOO^-$ scavenger, uric acid level in serum or CSF could reflect disease activity and correspond to therapeutic responses in MS patients [16, 17]. Peroxynitrite decomposition catalyst (PDC) or blocking $ONOO^-$ formation ameliorated acute and chronic relapsing in EAE [18, 19]. Thus, $ONOO^-$ could be a player in MS pathology. However, direct evidence is still lack whether $ONOO^-$ mediates mitophagy activation during MS/EAE pathology.

Dynamin-related protein 1 (Drp1) is a key factor in regulating mitophagy. Drp1 is recruited to the damaged mitochondria and triggers mitochondrial fission/fragmentation, subsequently facilitating mitophagy induction [20]. Dysfunction of Drp1 contributes to excessive mitochondrial fragmentation, leading to synaptic damage and neuronal loss [21]. Drp1 inhibitor abolished Drp1 translocation to mitochondria and attenuated mitochondrial fragmentation and EAE progress [22]. Posttranslational modifications of Drp1 could regulate mitochondrial fission. Nitrosative stress appears to promote Drp1 translocation and mitochondrial fragmentation. S-nitrosylation of Drp1 could mediate beta-amyloid mitochondrial fission and neuronal injury [21]. NO induces S-nitrosylation of Drp1, linking excessive mitochondrial fission and contributing to neuronal injury [23]. Notably, the nitration of mitochondrial proteins have been reported to induce mitochondrial dysfunction, apoptosis and neurodegeneration in EAE animal model [24]. We recently reported that $ONOO^-$ production induced the recruitment of Drp1 into the damaged mitochondria and activated mitophagy in cerebral ischemia-reperfusion injury [25]. Thus, we raise the question about the roles of the $ONOO^-$ -mediated mitophagy in MS/EAE pathology. If it is the case, how $ONOO^-$ initiates the recruitment of Drp1 into the mitochondria would be a critical question for understanding the molecular mechanisms of the MS/EAE pathology. In the present study, we aim to explore the potential function of nitrative-modified Drp1 as a mitophagy activator during EAE pathogenesis. Our results demonstrate that $ONOO^-$ could be a critical factor in EAE development through inducing nitration of Drp1 for the

mitochondrial recruitment, subsequently triggering mitophagy activation and aggravating axonal degeneration and neuronal injury.

2. Materials and methods

2.1. Animals

Female C57BL/6N mice (10-14week old) and fetal Sprague-Dawley rats (embryonic days E17-18 day) were obtained from the Laboratory Animal Unit, the University of Hong Kong. All animal care and experimental procedures were approved by the University Committee on the Use of Live Animals in Teaching and Research (CULATR). Animals were housed in the pathogen free environment with 12 hours dark/light cycles.

2.2. Active EAE induction.

Female C57BL/6N mice were immunized for active induction of EAE as our previous described [26]. Briefly, the mice were subcutaneously injected with 200μg $MOG_{35–55}$ in complete Freund's adjuvant (5 mg/ml, Sigma-Aldrich). *Pertussis Toxin* (200 ng, List Biological Laboratories) was injected intravenously twice on 0 and 2 days postimmunization (dpi.). The immunized mice were monitored daily with body weight measurement and clinical scores evaluation. EAE symptoms were scored daily as follows: 0, no clinical signs; 0.5, partially limp tail; 1, paralyzed tail; 1.5, hindlimb paresis or loss in coordinated movement; 2, loss in coordinated movement and hindlimb paresis; 2.5, one hindlimb paralyzed; 3, both hindlimbs paralyzed; 4, hindlimbs paralyzed, weakness in forelimbs; 5, forelimbs paralyzed.

2.3. Experimental Groups and Drug Treatment

To investigate the roles of autophagy/mitophagy in neuronal injury and disease severity at acute phases of active EAE mice, we designed parallel groups including vehicle control, EAE, and EAE treated by autophagy inhibitor 3-methyladenine (3-MA, M9281; Sigma, MO, USA) and mitochondrial division/mitophagy inhibitor mdivi-1 (M0199; Sigma). Female C57BL/6N mice were divided into sham control,

EAE-vehicle, EAE plus 3-MA or mdivi-1 groups (n=8-12). 3-MA (75mg/kg/day), mdivi-1 (50 mg/kg/day) or vehicle (saline) were administered intraperitoneally from the disease onset (11 dpi) for 7 consecutive days.

To examine the roles played by $ONOO^-$ in EAE pathology, we used FeTMPyP, a representative peroxynitrite decomposition catalyst (PDC). In the experiments, FeTMPyP (20 mg/kg/day, n=8-12) or vehicle (saline) were intraperitoneally injected into EAE mice started at onset of disease (11 dpi) continuously for 7 days. Body weights and clinical scores were daily evaluated.

2.4. Cell Culture

Human neuroblastoma SH-SY5Y cell line was purchased from ATCC (Catalog CRL-2266™). SH-SY5Y cells were cultured in high-glucose Dulbecco's modified Eagle's medium (DMEM) with 10% fetal bovine serum, 1% L-glutamine, plus 1% penicillin and streptomycin. Each medium was purchased from Gibco, Life Technologies (Carlsbad, CA, USA).

Primary rat motor neuron was prepared from the cortex of fetal Sprague-Dawley rats (embryonic days E17-18 day), as described previously [27, 28]. Briefly, neurons were dissociated from the cerebral cortex of embryonic rats, digested with accutase (Thermo Fisher, USA), filtered into single cells with strainer and seeded on microscope slides pre-coated with Poly-D-Lysine (Sigma-Aldrich, USA). Cells were maintained in neurobasal medium supplement with 2% B27 (Life technologies, USA). At 24 hours after seeding, the cultured medium was supplemented with 1 μM cytosine arabinoside (Cayman Chemical, USA) to suppress the proliferation of glia. At day 2, half of the culture medium was changed twice per week and the cells were cultured at 37 °C in a 95% O_2 and 5% CO_2 humidified incubator for at least 7 days.

2.5. Cell Treatment

We explored the causal link between $ONOO^-$ production and mitophagy activation in neurons. SH-SY5Y cells or primary neurons were exposed to $ONOO^-$ donor synthesized sodium peroxynitrite (81565; Cayman) to induce the nitrative stress *in vitro*. Specifically, the cells were treated with 20, 40, and 80 μM sodium

peroxynitrite respectively for 2 h. In PDC treatment group, FeTMPyP (50 μM) was added into the culture medium when the cells were challenged by sodium peroxynitrite (80 μM). The samples were collected for western blot, immunofluorescence or/and TEM studies.

2.6. Plasmid and Cells Transfection

The plasmid mCherry-Drp1 was purchased from Addgene (#49152). Escherichia coli with the plasmid were grown in LB medium at 37°C overnight with 50 mg/ml kanamycin. The plasmids were extracted by QIAGEN Plasmid Mini Kit (Cat No./ID: 12125).

To visualize Drp1, SH-SY5Y cells were transformed with Dnm1-mCherry. In detail, SH-SY5Y cells (4×10^5 cells/ml) were seeded in a 20mm confocal dish (MatTek) for 24 h before transfection. Then, 0.5 μg Dnm1-mCherry plasmids were transfected in OPTI-MEM media (Invitrogen) with 5 μL Lipofectamine 2000 (Invitrogen) per well for 48h. After received different treatments, the live cells were imaged over time by a confocal laser scanning microscope LSM 800 (Carl Zeiss).

2.7. Mitochondrial Isolation

Mitochondrial isolation was performed by using a commercial mitochondria isolation kit (89801; Thermo, IL, USA). In detail, the mouse spinal cord was dissociated and the tissue was carefully triturated into homogeneous suspension with a glass homogenizer. Mitochondria were separated from cytosolic fraction by using extraction reagents and differential centrifugation. Mitochondrial protein was extracted with 2% CHAPS (C9426; Sigma) in Tris-buffered saline (TBS). Then, mitochondrial and cytosolic proteins were collected respectively for further study. Western blot analysis was performed to determine the integrity and purity of isolated mitochondria by using mitochondrial marker VADC1/porin (ab15895; Abcam, Cambridge, UK).

2.8. TUNEL Assay

Apoptotic cell death was detected by terminal deoxynucleotidyl transferase-mediated dUTP nick end labeling (TUNEL) assay. Briefly, isolated L4-L6

spinal cord was collected at the peak time of the disease (18 dpi) and fixed with 4% paraformaldehyde (PFA). After dehydrated in gradient ethanol and permeabilized with xylene, the tissues were embedded into paraffin and cut into 5 μm sections. Slides were stained with TUNEL reagents (Roche Diagnostics, IN, USA) for labelling apoptotic cells and DAPI for marking nucleus. The fluorescent images were observed by using a confocal laser scanning microscope LSM 800 (Carl Zeiss).

2.9. Peroxynitrite assessment

We developed and patented a series of fluorescent probes for $ONOO^-$ detection with high selectivity and sensitivity, including HKYellow, HKYellow-AM and MitoPN-1 [29-31] (U.S. 11848-027-999; WO2013113279A1). Those probes were used to detect the levels of $ONOO^-$ in serum and CNS tissues. The dynamic changes of $ONOO^-$ in the serum of EAE mice at different time points (0, 5, 10, 15, 20, 25 and 30 dpi) were detected by HKYellow probe. Detailly, HKYellow (10 μM, 1mL/kg) were intravenously injected into the mice at 5 min prior to serum collection. The serum was transferred to 96-well black plates and the fluorescent intensity was determined at an excitation wavelength of 543 nm and emission wavelength of 567 nm by using a spectrofluorometer (Lambda55, PerkinElmer). The relative $ONOO^-$ concentration in EAE mice was calculated by comparing with sham mice with the formula $[(A_{EAE}-A_{sham})/ A_{sham}]*100\%$.

To detect $ONOO^-$ levels in CNS, as previous described, we intravenously injected HKYellow-AM (10 μM, 1mL/kg) or MitoPN-1(100 nM, 0.01mL/kg) into the mice at 18 dpi at 15 min before sacrificed. After perfused with PBS, fresh L4-L6 spinal cords were immediately dissected out, embedded into O.T.C., cut into 30 um sections, counterstained the nucleus with DAPI. Mitochondrial $ONOO^-$ production was detected by using MitoPN-1. The tissue sections were post-fixed for 30 min before embedding process and then co-stained with neuron marker MAP-2 and 3-nitrotyrosine (3-NT, an $ONOO^-$ footprint marker). Images were captured by a confocal laser scanning microscope LSM 800 at an excitation wavelength of 543 nm/emission wavelength of 567 nm.

2.10. Immunoprecipitation

Total Drp1 proteins in mice spinal cords or SH-SY5Y cells were pulled down by Dynabeads using Dynabeads® protein G immunoprecipitation kit (10007D, Novex, Life Technologies) according to manufacturer's instructions. In brief, samples were incubated with 50 µL Dynabeads and then Drp1 primary antibody (Cell Signaling Technology, 8570) in 200 µL antibody (Ab) binding and washing buffer for 30 min at RT. After removed supernatant and washed Dynabeads, the extracted sample containing 500 µL antigen (Ag)-containing protein was incubated with the Dynabeads-Ab complex for 2 h under rotation. The supernatant was collected as the flow-through sample by using a magnet after washed three times. The washed Dynabeads-Ab-Ag complex was gently eluted as the target Drp1 sample for western blot analysis.

2.11. LC-MS/MS analysis

The spinal cords from EAE mice (18dpi) were suspended in the RIPA lysis buffer. The proteins were extracted from cell lysate by using Precellys homogenizer followed by centrifugation at 15000 g for 25 min at 4 ^{o}C. Supernatant fraction was collected for protein quantitation by using BCA assay. Briefly, 200 µg proteins were subjected to trypsin digestion following reduction and alkylation by using Filter-Aided Sample Preparation (FASP) method. LysC-Tryptic peptides were cleaned by using C18 stage tips and speedvac dried. To enhance the proteins coverage, the peptides from each sample were fractionated with the High pH Reversed Phase Peptide Fractionation Kit (Thermo) into 4 concatenated fractions. The eluted peptides were desalted using C18 ZipTips before submitting for LC-MS/MS analysis.

For MS/MS processing, the eluted peptides were analysed with Dionex Ultimate 3000 nanoRSLC system coupled to Thermo Fisher Orbitrap Fusion Tribid Lumos. The peptides were separated on commercial C18 column (75 µm i.d. × 50cm length) with 1.9 µm particle size (Thermo Fisher). Separation was attained by using a linear gradient of increasing buffer B (80% ACN and 0.1% formic acid) and declining buffer

(0.1% formic acid) at 300 nL/min, and followed by 180 min analytical separation including 5% B for 10 min, a linear increase to 32% B at 148 min, 95% B wash from 158 to 168 min, and re-equilibration at 5% B from 169−180 min. Mass spectrometer was operated in positive polarity mode with capillary temperature of 300 °C. Full MS survey scan resolution was set to 120 000 with an automatic gain control (AGC) target value of 2×10^6, maximum ion injection time (IT) of 100 ms, and for a scan range of 350−1700 m/z. Higher-energy collisional dissociation (HCD) was used for operation in which a data-dependent top 10 method was selected. Spectra were obtained at 30000 MS2 resolution with 1×10^5 AGC target operated with the maximum ion injection time (IT) at 100 ms, isolation width at 1.6 m/z, and normalized collisional energy at 30. Preceding precursor ions targeted for HCD were dynamically excluded for 50 s.

For data analysis, Maxquant version 1.6.3.3 was adopted, in which the high resolution and high mass accuracy MS data analysed in triplicates were searched using the Andromeda algorithm against Mouse UniProt FASTA database. Nitration was selected as modifications with a nitrated residue as a mass increase of 44.985 Da. Confident proteins were identified by using a target-decoy approach with a reversed database, strict false-discovery rate <0.001 at peptide and PSM level.

2.12. Histopathology

Luxol fast blue (LFB) was employed for the assessment of demyelination and evaluation of histological severity during EAE pathology. In detail, isolated L4-6 spinal cords at different phases (0, 11, 18, 30 dpi) were post fixed in 4% PFA, dehydrated in gradient ethanol, embedded into paraffin and cut into 5μm sections. For Luxol fast blue (LFB) staining, slides were rinsed in 95% alcohol, stained with 0.1% luxol fast blue solution (0.1g LFB powder, 0.5% glacial acetic acid in 95% alcohol) at 60°C overnight. Rinse slides in 95% ethyl alcohol and differentiated in 0.05% lithium carbonate solution for 30-40 seconds and 70% ethyl alcohol until white matter and grey matter were sharply defined. Counterstained the sections with 0.1% cresyl violet for 10-20 seconds. The myelin in the white matter should be blue which can sharply

distinguish from the demyelination areas.

2.13. Transmission electron microscopy (TEM)

Isolated lumbar spinal cords were cut into 1.0 mm thick sagittal block and fixed in EM fixative (2% PFA and 2.5% glutaraldehyde in 0.01M PB solution) at 4°C for 72-96 hours followed by post fixed in 1% osmic acid at 4°C overnight. Then, the blocks were dehydrated in graded ethanol, infiltrated in propylene oxide (P.O.), embedded into EPON, polymerized and cut into 90 nm ultrathin sections with 3% uranyl acetate and 1% lead citrate staining. Digital images were captured by electron microscopy (TEM, Phillips CM100).

Recombinant human Drp1 protein (Abcam, 153041) was diluted to 5 μg/ml in buffer (20 mM Hepes pH 7.4, 100 mM NaCl, 1 mM $MgCl_2$) and treated with or without fresh synthesized sodium $ONOO^-$ (80 μM) for 10 min on ice and protected from light. To obtain oligomerization, protein samples were incubated with 1 mM GTP for about 30 min at RT. Samples were adsorbed to carbon-coated copper EM grids, negatively stained with 1% uranyl acetate, air dried and imaged with a FEI Tecnai G2 20 Scanning TEM (FEI) at an accelerating voltage of 120 kV and equipped with an AMT XR80C CCD camera (Advanced Microscopy Techniques, NJ).

2.14. Immunofluorescence Staining

Post-fixed tissues were immersed in 30% sucrose solution at 4°C for complete dehydration, embedded in O.C.T, cut into 30 μm sections as frozen slices and stored at -20°C. For immunofluorescence *in vitro*, cells were seeded onto 12 mm microscope slides (0111500; GmbH & Co. KG, Germany). After different experiment, cells were fixed in 4% PFA for 20 minutes at RT and stored at 4°C in PBS. For immunostaining, the epitopes of frozen slice samples were retrieved with 10 mM sodium citrate buffer (pH=6.0) by using the microwave oven for 30 min. Then, after washed by PBS, the sections or cells were blocked in 5% goat serum, incubated with primary antibodies, stained with fluorochrome conjugated secondary antibodies, counterstained the nucleus with DAPI and mounted with antifade medium (Dako). Immunofluorescent images were visualized using a confocal laser scanning microscope LSM 800 (Carl

Zeiss). All antibodies were listed in Supplementary Table 1.

2.15. Direct Stochastic Optical Reconstruction Microscopy

We then directly visualized the protein-protein interactions and their colocalization by using direct stochastic optical reconstruction microscopy (dSTORM). We detected the nitration of Drp1 by co-staining Drp1 with 3-NT expression in the 5 μm-paraffin sections isolated from L4-L6 spinal cords from control or EAE mice at 18 dpi *in vivo*. We also performed *in vitro* experiments to further understand the direct effects of $ONOO^-$ on mediating mitochondrial translocation of Drp1 in SH-SY5Y cells. After challenged by $ONOO^-$ exposure, the cells were co-stained Drp1 with HSP60, a mitochondrial marker. The slices or coverslips were incubated with immediately dissolved image buffer (1ml including: 350μl MilliQ H_2O, 500μl 20% Glucose, 50μl 1M Tris-HCl 8.0, 50μl 0.5M TECP, 10μl 200mM Cyclooctatetrane, 10μl 100mM Ascorbic acid, 10μl 100mM Methyl Viologen, 10μl 65mg/ml Glucose oxidase and 10μl 4mg/ml Catalase), which fulfilled in the chamber with the coverslip under the bottom. Chamber was placed under the 100x oil objective to process the image acquisition. Wide field images were obtained beforehand. Followed by calibrating the position based on the beads, super-resolution progress then was performed under the Lunar software.

2.16. Live imaging by confocal microscopy

To detect the mitochondrial translocation of Drp1, the mCherry-Drp1-transfected SH-SY5Y cells were grown on glass-bottom MatTek dishes and stained with Mito-tracker Green FM (Invitrogen) at 37°C for 15min. Then, dishes were loaded to a Wave FX spinning disk confocal microscope (Quorum Technologies) on an Eclipse Ti microscope (Nikon) equipped with Hamamatsu ImageM EM CCD cameras and Bionomic Controller (20/20 Technology) with temperature-controlled stage at 37°C. After equilibrating to temperature for 10 min, cells were treated with freshly prepared $ONOO^-$ (80 μM final concentration on cells) during imaging. The cells were imaged with the 488-nm laser and 525/30 filter for Mito-tracker, 561-nm and 595/25 for mCherry on a confocal laser scanning microscope LSM 800 (Carl Zeiss).

2.17. GTPase Assay

The GTPase enzymatic activity of Drp1 was measured using a Novus Biological calorimetric kit (Littleton, CO, USA) as previous described [32-34]. Based on Drp1 hydrolyzing GTP to GDP and inorganic phosphorous (Pi), GTPase activity was evaluated by measuring the amount of produced inorganic Pi. Then, by adding the ColorLock Gold (orange) substrate, the orange complex reacted with the Pi and generated to form inorganic complex solution (green). Calorimetric measurements (green) were read in the wavelength range of 650 nm. We detected GTPase Drp1 activity in the lysates of spind cord tissues from control mice and active EAE mice (18dpi). In detail, spinal cords were excised, homogenized in PBS with protease inhibitors, added Triton X-100 to a final concentration of 1% and frozen at -80° C overnight. Then, the frozen samples were thaw and centrifuged at 10,000 x g for 15 minutes to remove cellular debris and collected the supernatant. Sample protein concentrations were quantified by using a total protein assay. For *in vitro* detection of GTPase Drp1 activity in recombinant Drp1 and $ONOO^-$-treated Drp1, Drp1 proteins were pre-incubated with or without synthesized sodium $ONOO^-$ (80 μM final working concentration) for 10 min on ice to induce Drp1 nitration. In a GTPase assay, according to the manufacturer's instructions, 100 μl equal amounts of proteins were added 96-well plates, added 100 μl substrate/buffer for 5-90min, added 50 μl of Pi ColorLock mix to stop reactions, added 20μl of Stabilizer for 30 min and read the plate at a wavelength in 650 nm.

2.18. Western blotting

Following different experimental conditions, protein samples from tissues or culture cells were extracted by using radioimmunoprecipitation assay (RIPA) buffer containing 1% proteinase and phosphatase inhibitor cocktails (Sigma-Aldrich). Mitochondrial and cytosolic proteins from mouse spinal cords were prepared after mitochondrial isolation. For oligomeric/ polymeric Drp1 detection, the samples were processed without reductant and dithiothreitol (DTT). All procedures were referred to the standard western blot protocol. After protein quantification, equal amounts of

proteins were applied and separated in SDS-PAGE, electronic transferred onto polyvinylidene difluoride (PVDF) membranes (0.45um pore size, Millipore, CA, USA), blocked with 5% bovine serum albumin overnight at 4 ℃ and immunoblotted with primary antibodies following HRP-conjugated secondary antibodies (Supplementary Table 1). The signals were detected by chemiluminescent ECL Select Kit (GE Healthcare, IL, USA), captured by Gel-Doc system (Bio-Rad, CA, USA) and analyzed by Image Lab software (Bio-Rad, CA, USA).

2.19. Statistical analysis

Data were expressed as the Mean ± S.E.M. Statistical analysis was assessed by using unpaired Student's t test for two group designed comparisons or One-way ANOVA followed by Dunnett's multiple-comparison test for multiple group comparisons. The numbers of mice used are described in the corresponding figure legends and all experiments were repeated three or more times. All data were performed using GraphPad Prism Version 6.0 software (GraphPad Software Inc., CA, USA). A value of $p < 0.05$ was considered statistically significant.

3. Results

3.1. Inhibition of autophagy activation attenuates EAE symptoms.

Basal autophagy maintains cellular homeostasis by removing damaged components for survival whereas activated autophagy aggravates axonal destruction and leads to cell death [4, 5, 35]. Thus, we first sought to detect dynamic levels of autophagy at different phase of EAE pathological progression. We collected spinal cords from EAE mice at 0, 11, 18 and 30 dpi, corresponding to the time points of initial injection, the disease onset, the peak and the recovery phase respectively. As shown by LFB staining and TEM imaging (Fig. 1A), the EAE mice had the remarkable increased demyelination in spinal cords at the peaktime of disease progresses (18 dpi). The EAE mice had the enhanced expression of amyloid precursor

protein (APP) and the decreased ratio of bcl-2/Bax in the spinal cords, indicating the axonal damage and cell death respectively (Fig. 1B). At the disease peaktime (dpi 18), the EAE mice had peak levels of axonal damages, cell death, body weight loss and clinical deficit scores. Consistently, TUNEL staining showed that the EAE mice had elevated apoptotic cell death in the spinal cords at 18dpi (Fig. 1C). Simultaneously, the increased LC3-II/I, an autophagosome marker, was found in the spinal cords of the EAE mice at 18 dpi (Fig. 1B). We then identified the neuronal autophagy by co-staining LC3 with a neuronal marker Tuj1. Compared with the control group, the EAE group (18 dpi) had an obvious change in the distribution of LC3, showing the cytosolic LC3 aggregation to form puncta in the neurons of spinal cords (Fig. 1D). These results suggest that the activated neuronal autophagy could be coincident with the severities of axonal degeneration, neuronal cell death and disease progression in the spinal cords of the active EAE mice.

We next investigated the effects of autophagy inhibitor 3-MA on the disease severity in EAE mice. Since autophagy activation was gradually enhanced starting from the disease onset, we injected 3-MA (75mg/kg/day) intraperitoneally into EAE mice started at 11 dpi continuously for 7 days. Treatment of 3-MA attenuated the loss of body weight and alleviated clinical scores in the active EAE mice (Fig.1 E-G). Those results suggest that the activated autophagy might contribute to CNS damages and disease progression in EAE pathology. Considering the synchronism between autophagy and disease severity in EAE, we collected all tissues from the EAE mice at peak of disease (18dpi) for further study.

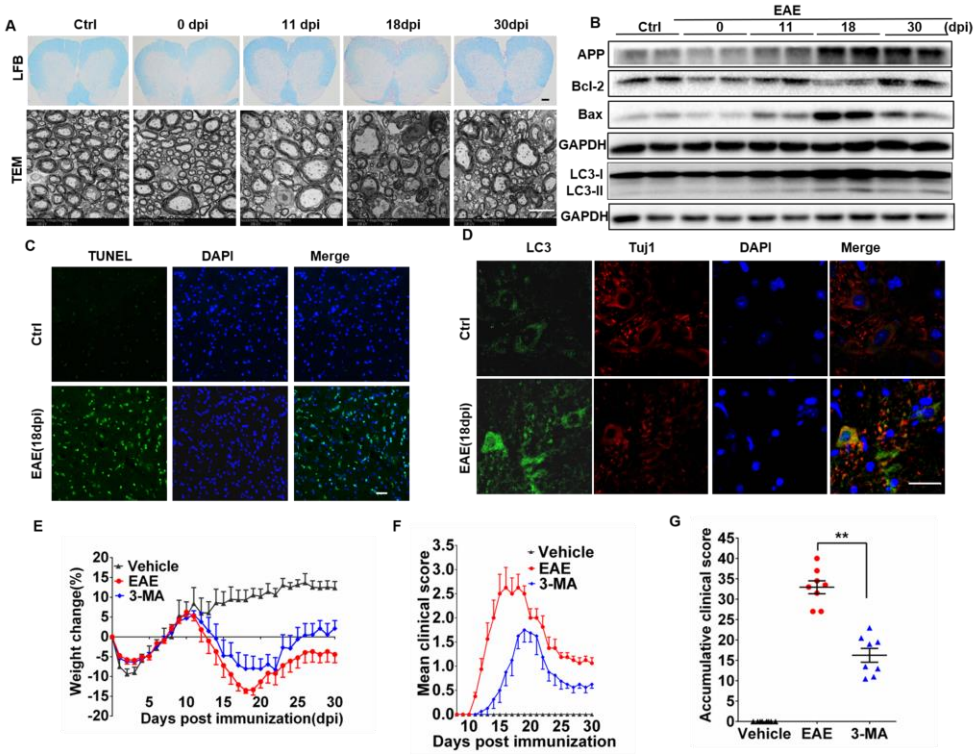

Fig 1. Autophagy level was obviously increased accompanying with axonal degradation and neuronal cell death and autophagy inhibitor 3-MA alleviated EAE symptoms. (A) Histological examination of demyelination in the lumbar spinal cords (L4-L6) of control and active EAE mice by Luxol fast blue (LFB) staining (scalebar,100μm), and electronic microcopy (scalebar, 5μm) at different phases (0, 11,18 and 30 dpi). **(B)** Western blot detection of the time-dependent response of APP, Bcl-2, Bax and LC3I/II expressions in spinal cord of immunized EAE mice. **(C)** TUNEL assay of lumbar spinal cords in vehicle or active EAE mice at peak of disease (18dpi). Scale bars, 50 μm. **(D)** Immunofluorescent co-staining of LC3 with Tuj1 in the gray matter of spinal cords of immunized EAE mice (18dpi). Scale bars, 50 μm. **(E)** Mice received treatments of vehicle (n=8) or 3-MA (75 mg/kg/day, n=8) by i.p. starting from day 11 after EAE induction for 7 days consecutively. The body weights were evaluated daily for up till day 30 post immunization. **(F)** Clinical scores of vehicle, active EAE or 3-MA treated mice after immunization. **(G)** Accumulative clinical scores of vehicle, active EAE or 3-MA treated mice for 30 dpi. **p<0.01 was determined by one way ANOVA followed by Newman Keuls test.

3.2. PINK1/Parkin-mediated mitophagy is activated via recruiting Drp1 into damaged mitochondria in EAE pathology

Mitochondrial recruitment of Drp1 is essential for the initial step of mitochondrial fission/fragmentation, and PINK1/Parkin pathway subsequently regulates the mitophagic process to degrade damaged mitochondria in most cases [36, 37]. To

detect mitophagy, we isolated cytosol and mitochondrial fractions from spinal cords of the EAE mice. We found that the ratio of LC3-II/LC3-I was markedly increased in mitochondrial fraction isolated from the EAE mice (18dpi) when compared with the total protein extraction (Fig. 2A). Electron microscopy imaging revealed the obviously damaged mitochondria with blurry ruptured cristae and extensive mitochondrial fragmentation in the spinal cords of the EAE mice (Fig. 2B). Western blot results showed that Parkin translocation from cytoplasm to mitochondria was companied with the increased PINK-1 expression in mitochondrial outer membrane (MOM) and the enhanced Drp1 recruitments into mitochondria (Fig. 2C). Consistently, immunofluorescence revealed that LC3 was evenly distributed in the cytoplasm of the control group, whereas intensive LC3 puncta was aggregated to mitochondria marked by ATPB in the spinal cords of EAE mice (18dpi) (Fig. 2D). By co-staining of Drp1 and ATPB, we also found that Drp1 was translocated into the mitochondria in the samples from the EAE mice, suggesting that mitophagy could be activated in Drp1 and Parkin dependent manners (Fig. 2E). Besides, by using co-immunostaining of TuJ1 and Drp1, we found that the Drp1 mitochondrial translocation was associated with mitophagy activation in neurons of the EAE-induced spinal cords (Supplementary Fig.1). These results suggest that mitophagy, as a selective autophagy, might dominate in the neurons of the EAE mice.

To identify the roles of Drp1 in mitophagy activation for EAE pathogenesis, we treated the EAE mice with Mdivi-1, a selective Drp1 inhibitor. Treatment of Mdivi-1 attenuated pathological symptoms, postponed disease progression, and alleviated clinical scores in the active EAE mice (Fig. 2F-H). The Mdivi-1 administration suppressed the translocation of Drp1 and Parkin into the mitochondria, decreased mitochondrial PINK1 expression and inhibited mitophagy activation with the reduced ratio of mitochondrial LC3-II/LC3-I in the spinal cords of the EAE mice (18dpi) (Fig. 2I). These results, when taken together, indicate that Drp1 recruitment into mitochondria plays crucial roles in PINK1/Parkin-mediated mitophagy activation, contributing to EAE symptomatic aggravation.

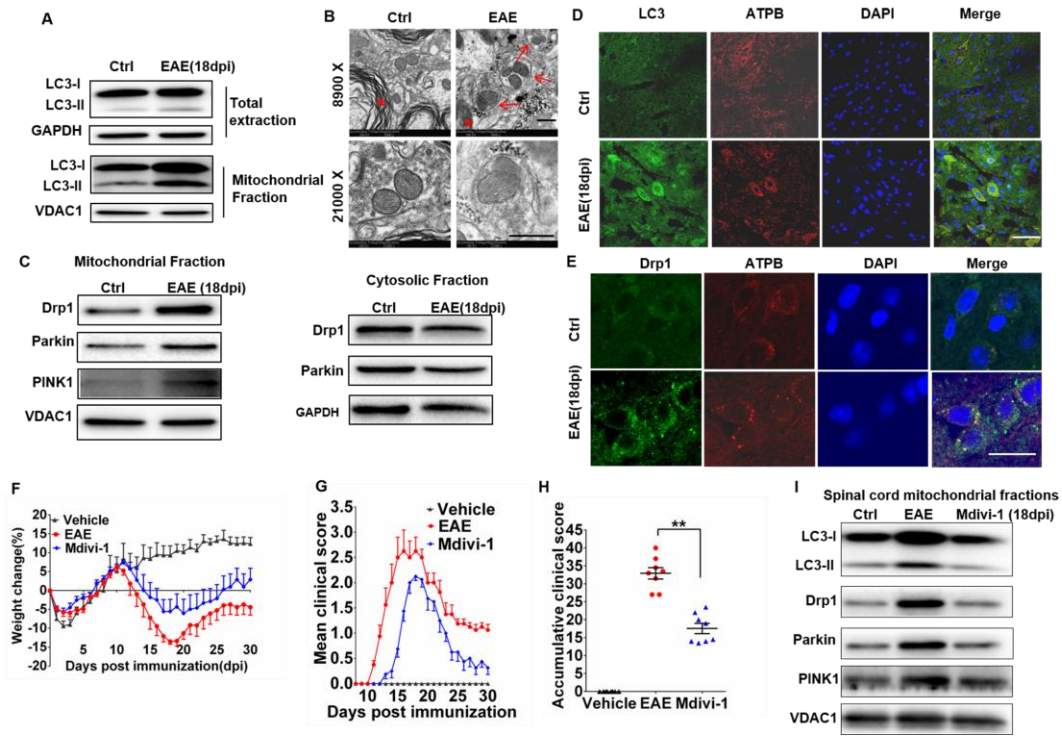

Fig 2. PINK1/Parkin-mediated mitophagy was dominated with mitochondrial recruitment of Drp1 in spinal cords of active EAE mice, which was reversed by Drp1 inhibitor Mdivi-1 with attenuating EAE progression. **(A)** Western blot detection for the ratio of LC3-II/LC3-I in total and mitochondrial fractions from the lumbar spinal cords in vehicle or active EAE mice (18 dpi). **(B)** The ultrastructure of axon, myelin sheath or mitochondria in the gray matter of lumbar spinal cord regions (L4-L6) (18 dpi) was evaluated by transmission electron microcopy (TEM). Asterisk pointed the myelin; Arrow for mitochondria. Scale bars, 200 nm. **(C)** Western blot detection for involved protein expression levels in mitochondrial and cytosolic fractions isolated from spinal cord tissues (18dpi). **(D)** Immunofluorescent co-staining of LC3 with ATPB in the gray matter of spinal cords of immunized EAE mice (18dpi). Scale bars, 50 μm. **(E)** Immunofluorescent co-staining of Drp1 with ATPB in the gray matter of spinal cords of active EAE mice(18dpi). Scale bars, 50 μm. **(F)** Mice received treatments of vehicle (n=8) or Drp1 inhibitor Mdivi-1 (50 mg/kg/day, n = 8, i.p. started at 11 dpi for 7 days). The body weights were evaluated daily for up till day 30 post immunization. **(G)** Clinical scores of vehicle, active EAE or Mdivi-1-treated mice after immunization. **(H)** Accumulative clinical scores of vehicle, active EAE or Mdivi-1-treated mice for 30 dpi. **p<0.01 was determined by one way ANOVA followed by Newman Keuls test. **(I)** Western blot detection for the ratio of LC3-II/LC3-I and involved proteins in mitochondrial fractions from spinal cords in vehicle, active EAE or Mdivi-1-treated EAE mice (18 dpi).

3.3. $ONOO^-$ triggers Drp1 mitochondrial recruitment and induces mitophagy activation during EAE pathology

To elucidate the roles of $ONOO^-$ in mitophagy activation during EAE pathogenesis, we detected the dynamic changes of $ONOO^-$ production in the period of active EAE. Interestingly, by using our extracellular $ONOO^-$ probe HK-Yellow, we found that the elevated serum $ONOO^-$ level was coincident with axonal damages, clinical scores and disease progression, which was reached to the peak level simultaneously with the disease severity at 18 dpi in the active EAE mice (Fig. 3A). ELISA assay showed that the trend of serum NT levels was similar to $ONOO^-$ production (Supplementary Fig. 2). In line with the increased $ONOO^-$ level in peripheral serum, we found the increased expressions of iNOS, NADPH oxidase subunit p47 phox and p67 phox, as well as 3-NT in the spinal cords of the active EAE mice (Fig. 3B). We further confirmed the increased $ONOO^-$ production in mitochondria of the neurons by co-staining MitoPN-1 (a mitochondrial specific $ONOO^-$ probe) with neuronal marker MAP-2 in the spinal cord of the active EAE mice (18dpi) (Fig 3C). These results indicate the increased $ONOO^-$ production in both peripheral serum and CNS during EAE pathology.

To explore the roles of $ONOO^-$ in mediated mitophagy activation, we injected FeTMPyP, a representative peroxynitrite decomposition catalyst (PDC) intraperitoneally into the EAE mice started from 11 dpi until to 18 dpi. As showed in Fig. 3D-F, PDC treatment prevented body weight loss and alleviated neurological deficit scores. Simultaneously, PDC treatment inhibited 3-NT expression and remarkably decreased intracellular $ONOO^-$ level in the spinal cords of the EAE mice (Fig. 3G, H). We further tested whether $ONOO^-$ was sufficient to induce mitophagy activation in the active EAE mice (18dpi). Western blot analysis revealed that the PDC treatment significantly reduced the ratio of LC3-II/LC3-I in mitochondria (Fig. 4A). The TEM study showed that the PDC-treated mice had less mitophagosome form and better mitochondrial structures with clear cristae in the spinal cords than the vehicle-treated EAE mice (Fig. 4B). Besides, PDC treatment suppressed the translocation of Drp1 and Parkin from cytosol to the mitochondria and reduced the expression of PINK1 in the mitochondria membrane obtained from spinal cords of the EAE mice. Immunofluorescent images showed that PDC intervention reversed LC3

puncta accumulation in the neurons and prevented Drp1 mitochondrial recruitment, as evidenced by co-immunostaining LC3 with ChAT, a motor neuron marker motor and Drp1 with ATPB respectively (Fig. 4C, D). Collectively, those results indicate that the $ONOO^-$ could mediate Drp1 mitochondrial recruitment and trigger neuronal mitophagy activation, subsequently aggravating disease progression in the EAE pathogenesis.

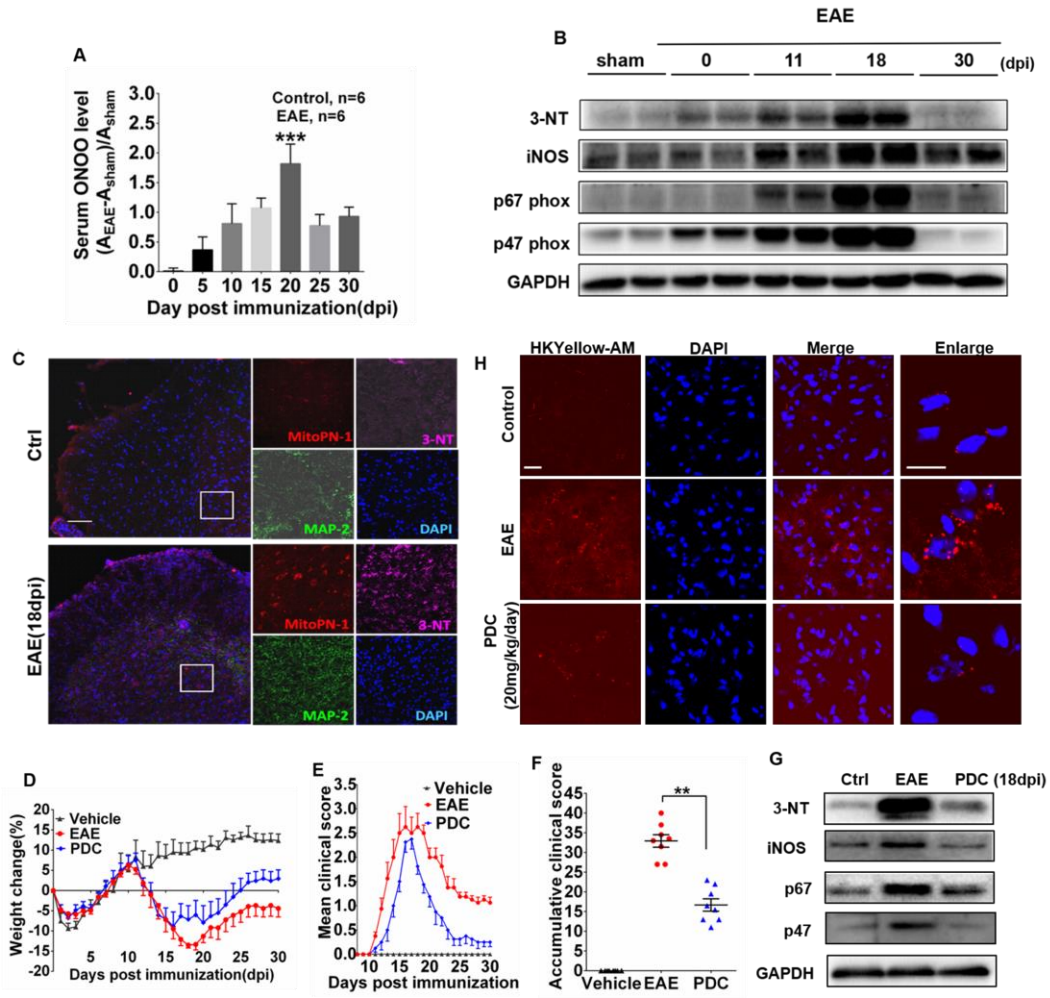

Fig 3. Peroxynitrite was largely generated in serum/spinal cords of active EAE mice, coinciding with EAE progression, which was attenuated by PDC. (A) Serum $ONOO^-$ levels detection in time-dependent active EAE mice after immunization by using HKyellow probe. **(B)** Western blot detection of 3-NT, iNOS, p67 phox and p47 phox expressions in spinal cords of active EAE mice at different phases. **(C)** Immunofluorescent co-staining of MitoPN-1 with 3-NT and MAP-2 in the gray matter of spinal cords of immunized mice(18dpi). Scale bars, 100 μm. **(D)** EAE mice were received vehicle (n=8) or PDC (20 mg/kg/day, i.p., n = 8) for 7 days. The body weights were evaluated daily for up till day 30 post immunization. **(E)** Clinical scores of vehicle, active EAE or PDC-treated mice after immunization. **(F)**

Accumulative clinical scores of vehicle, active EAE or PDC-treated mice for 30 dpi. **p<0.01 was determined by one way ANOVA followed by Newman Keuls test. **(G)** Western blot detection for the ratio of 3-NT, iNOS, p67 phox and p47 phox expressions in spinal cords of active EAE mice at different phases in vehicle, active EAE or PDC-treated EAE mice (18 dpi). **(H)** Immunofluorescent staining of HKyellow-AM in the gray matter of spinal cords of vehicle, immunized EAE or PDC-treated EAE mice (18 dpi). Scale bars, 50 μm.

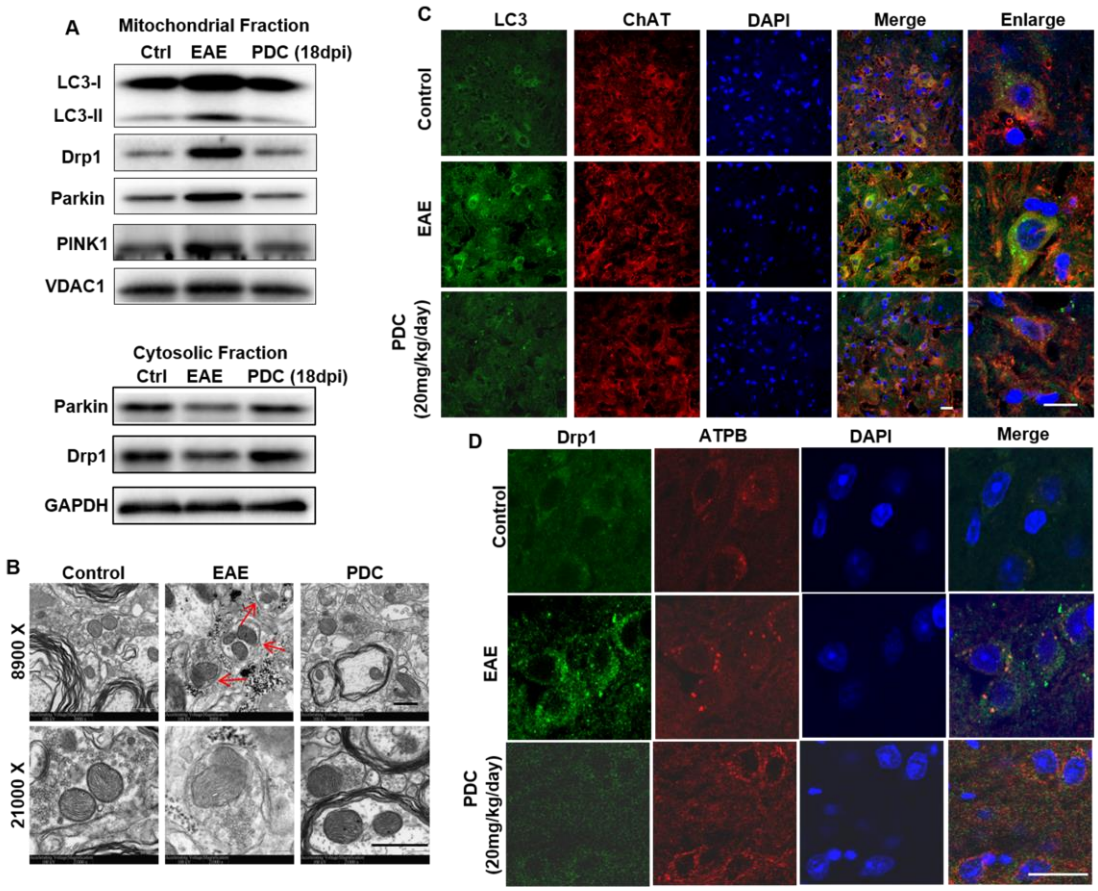

Fig 4. PDC treatment attenuated mitophagy activation via inhibiting mitochondrial recruitment of Drp1 in active EAE spinal cords. (A) Western blot detection for involved protein expression levels in mitochondrial and cytosolic fractions isolated from the spinal cord tissues of vehicle, immunized EAE or PDC-treated EAE mice (18 dpi). **(B)** The ultrastructure of axon, myelin sheath or mitochondria in the gray matter of lumbar spinal cord regions (L4-L6) from vehicle, immunized EAE or PDC-treated EAE mice (18 dpi) was evaluated by transmission electron microcopy. Arrow pointed the mitochondria. Scale bars, 200 nm. **(C)** Immunofluorescent co-staining of LC3 with ChAT in the gray matter of spinal cords of vehicle, active EAE or PDC-treated EAE mice (18 dpi). Scale bars, 50 μm. **(D)** Immunofluorescent co-staining of Drp1 with ATPB in the gray matter of spinal cords of vehicle, immunized EAE or PDC-treated EAE mice (18 dpi). Scale bars, 50 μm.

3.4. ONOO$^-$ triggers nitration of Drp1

We then tested how ONOO$^-$ triggered mitochondrial recruitment of Drp1 to induce mitophagy activation during EAE pathology. 3-NT blotting analysis following Drp1 immunoprecipitation (IP) revealed the increased ratio of the nitrated Drp1 to total Drp1 in the spinal cords of the EAE mice (18 dpi) (Fig. 5A, B). The results suggest the potential roles of ONOO$^-$ in mediating Drp1 nitration and translocation. Concomitantly, by using d-STORM imaging technology, we directly visualized the co-localization of Drp1 and ONOO$^-$ footprint marker 3-NT, indicating the nitrated Drp1 fluorescence in the spinal cords of the EAE mice (Fig. 5C). Furthermore, western blot study following Drp1 immunoprecipitation showed that PDC treatment group had remarkable lower the nitrated Drp1 level than the vehicle EAE group (Fig. 5D, E). Those results provide a clue that ONOO$^-$-mediated Drp1 nitration might initiate Drp1 mitochondrial recruitment in the spinal cords of the EAE mice.

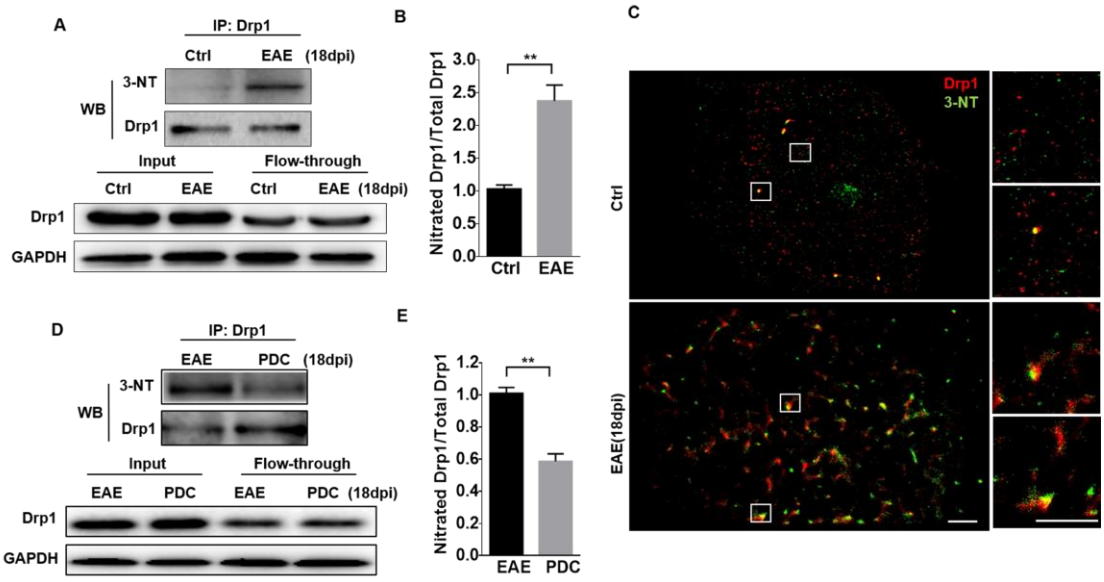

Fig 5. ONOO$^-$ triggered Drp1 nitration modification in the spinal cords of active EAE mice, which was reversed by PDC treatment. (A) Drp1 extracted from the spinal cords was pulled down and relatively purified by the immunoprecipitation method. Western blot detecting the ratio of nitrated Drp1 to total Drp1 in the vehicle and active EAE mice (18dpi) with 3-NT antibody. **(B)** Statistical analysis of **A**. (n=3) **(C)** Immunofluorescent co-staining of Drp1 with 3-NT in the gray matter of spinal cords of vehicle or immunized EAE mice (18 dpi) by dSTORM assay. Scale bars, 1 μm. **(D)** Western blot detection of Drp1 nitration level in active EAE mice and

PDC-treated EAE mice (18dpi) with 3-NT antibody. **(E)** Quantitative analysis of **D**. (n=3). Data are mean±SEM. **P<0.01, versus the EAE group, determined by unpaired Student's t test (**B** and **E**).

3.5. $ONOO^-$ donor initiates mitochondrial recruitment of Drp1 and mitophagy activation in vitro

We further conducted *in vitro* experiments to exclude the potential influences of other pathological factors and examine the exact roles played by $ONOO^-$ in mitophagy activation and neuronal cell death. SH-SY5Y cells was exposed to synthesized sodium $ONOO^-$ to induce nitrative stress *in vitro*. The $ONOO^-$ treatment dose-dependently increased LC3-II/LC3-I ratio and decreased in the expressions of bcl-2 (Fig. 6A). TUNEL staining experiment showed obviously apoptotic cell death in the SH-SY5Y cells after exposed to $ONOO^-$ challenge (Fig. 6B). Immunofluorescent staining study indicated that $ONOO^-$ treatment promoted the co-localization of LC3 puncta with ATPB and Drp1 with HSP60, a mitochondrial marker (Fig. 6C, D). Concomitantly, PDC treatment prevented the $ONOO^-$ mediated mitophagy activation and neuronal cell death.

We next examined the effects of $ONOO^-$ on mitochondrial division in the living SH-SY5Y cells transiently transfected with fluorescent marker for Drp1 (mCherry) and stained for mitochondria (mitotracer-green) by using fluorescence microscopy. The treatment of $ONOO^-$ led the Drp1 translocation and the puncta formation in the mitochondria where mitochondrial constriction and mitochondrial division events occurred over time (Fig. 6E). Thus, we concluded that $ONOO^-$ could trigger Drp1 mitochondrial recruitment and lead to mitochondrial division at that sites. Next, we determined the nitration of Drp1 and explored the roles of nitration of Drp1 in mediating mitochondrial division. Western blot analysis following Drp1 immunoprecipitation showed that $ONOO^-$ induced Drp1 nitration, whose effects were abolished by PDC treatment in SH-SY5Y cells (Fig. 6F, G).

Consistent results were also found in primary cultured neurons. Western blot analysis showed that $ONOO^-$ increased the ratio of LC3II/I and the expression of Bax in the cells (Fig. 7A, B). TEM study showed obvious fragmented mitochondria and

increased mitophagosome in the $ONOO^-$-treated neurons (Fig. 7C). Immunofluorescence study revealed that the $ONOO^-$ treated cells had LC3 accumulation in the mitochondria with marked by ATPB whereas the control cells had ubiquitous distribution of LC3 in cytosol (Fig. 7D). Similarly, Drp1 was revealed to form puncta around mitochondria under $ONOO^-$ condition (Fig. 7E). PDC treatment abrogated $ONOO^-$-induced excessive mitophagy activation and neurotoxic events. Those *in vitro* experiments confirm that $ONOO^-$ could be a player in activating Drp1-mediated mitophagy and aggravating neuronal cell death.

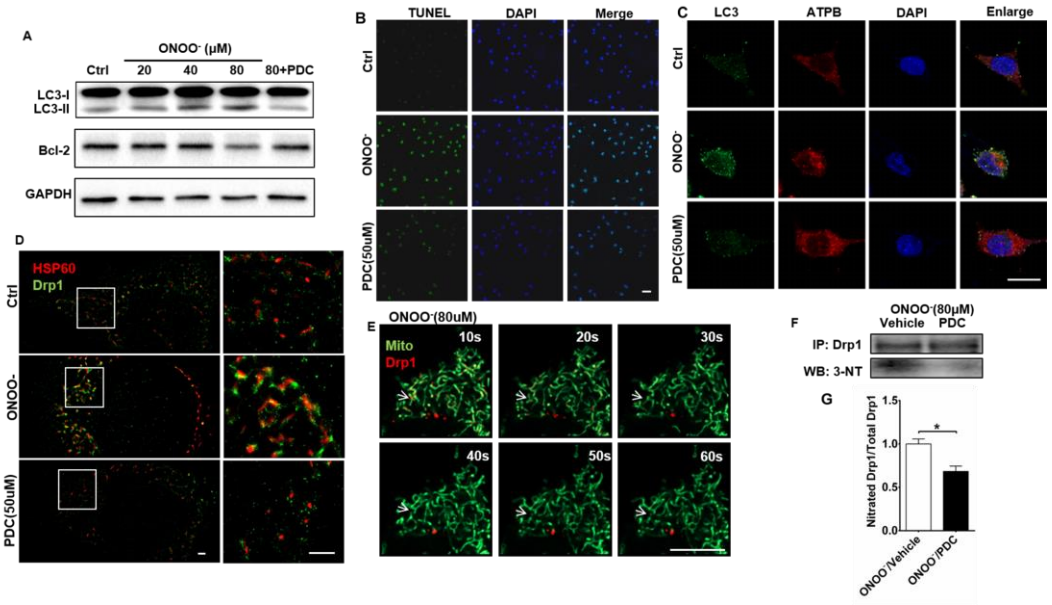

Fig 6. PDC inhibited Drp1 nitration and mitochondrial recruitment in SH-SY5Y cells exposing to peroxynitrite. (A) SH-SY5Y cells were exposed to synthesized sodium $ONOO^-$ for 2h to induce nitrative stress. Western blot images of cellular proteins involved in cell death (Bcl-2) and autophagy (LC3-II/LC3-I) in the groups of control, $ONOO^-$ (20, 40, and 80 uM), and $ONOO^-$ (80 μM) treated with PDC (50 μM). **(B)** TUNEL images of control, $ONOO^-$ (80 μM) and PDC-treated SH-SY5Y cells (50 μM). Scale bars, 20 μm. **(C)** Immunofluorescent co-staining of LC3 with ATPB in SH-SY5Y cells of control, $ONOO^-$ (80 μM) and PDC-treated groups (50 μM). Scale bars, 5 μm. **(D)** Immunofluorescent co-staining of Drp1 with HSP60 in SH-SY5Y cells of control, $ONOO^-$ (80 μM) and PDC-treated groups (50 μM) by dSTORM analysis. Scale bars, 1 μm. **(E)** Immunofluorescent co-staining of Drp1-mcherry with mitotracer-green in the time-dependent response to 80 μM $ONOO^-$ challenge on SH-SY5Y cells. Arrow pointed out the site that mitochondrial fission occurred. Scale bars, 1 μm. **(F)** Western blot images of nitrated Drp1 levels in $ONOO^-$ and $ONOO^-$ plus PDC groups with 3-NT antibody following Drp1 immunoprecipitation. **(G)** Statistical analysis of **F**. Data are expressed as mean±SEM. *P<0.05, versus the vehicle-$ONOO^-$ group (unpaired Student's t test).

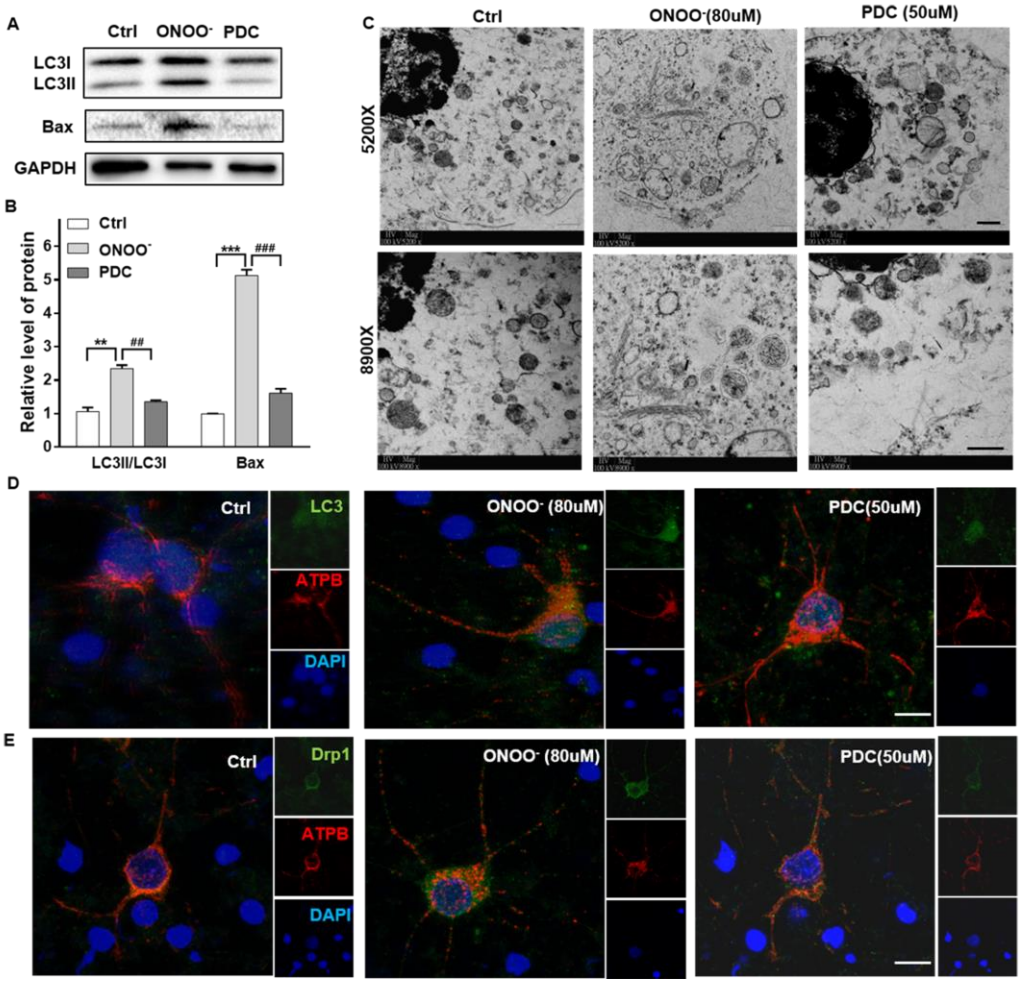

Fig 7. PDC inhibited ONOO$^-$ -induced mitophagy activation and suppressed Drp1 mitochondrial recruitment in primary cultured neurons. (A) Primary neuron isolated from rat cerebral cortex were exposed to synthesized sodium ONOO$^-$ (80 μM) for 2h to induce nitrative stress. Western blot images of cellular proteins involved in cell death (Bax) and autophagy (LC3-II/LC3-I) in the groups of control, ONOO$^-$ (80 μM), and ONOO$^-$ (80 μM) plus PDC (50 μM). **(B)** Statistical analysis of **A**. Data are expressed as mean±SEM. **P<0.01, ***P<0.001 versus the vehicle-ONOO$^-$ group (One-way ANOVA followed by Dunnett's multiple-comparison test). **(C)** The ultrastructure of mitochondria or autophagosome in primary neuron of control, ONOO$^-$ (80 μM) or PDC-treated groups (50 μM) was evaluated by transmission electron microcopy. Scale bars, 500 nm. **(D)** Immunofluorescent co-staining of LC3 with ATPB in primary neuron of control, ONOO$^-$ (80 μM) and PDC-treated groups (50 μM). Scale bars, 5 μm. **(E)** Immunofluorescent co-staining of Drp1 with ATPB in primary neuron of control, ONOO$^-$ (80 μM) and PDC-treated groups (50 μM). Scale bars, 5 μm.

3.6. Nitrative modification sites locate at GED domain of Drp1

We next sought to identify the target residues for nitration on Drp1. Orbitrap Fusion MS/MS analysis was performed on the spinal cords of EAE mice at 18dpi. Mass spectrometry data analysis revealed that two tyrosine in peptide sequences LIKSYFLIVR (Y 628) and AVMHFLVNHVKDTLQSELVGQLYK (Y 665) respectively were nitrative modification target points of Drp1 protein (Supplementary Fig. 3A, B). Sequence alignment of Drp1 demonstrated four distinct structural domains: a N-terminal guanosine triphosphatase (GTPase) domain, a dynamin-like middle domain, an insert B domain, and a C-terminal GTPase effector domain (GED). The nitrated peptide sequences both LIKSYFLIVR (Y 628 nitration) and AVMHFLVNHVKDTLQSELVGQLYK (Y 665 nitration) were located at GED of Drp1 (Fig. 8). The GED affects both GTPase activity and Drp1 oligomer/polymer formation, facilitating mitochondrial fission [38]. Drp1 self-assembly is a prerequisite in mitochondria dynamin [39, 40]. Dimers/tetramers Drp1 assemble to mitochondria and form rings, contributing to mitochondria fission due to physical forces and cooperative increased GTPase activity [41, 42]. Logically, the impacts of nitration of Drp1 on the Drp1 assembly or GTPase activity should be further explored.

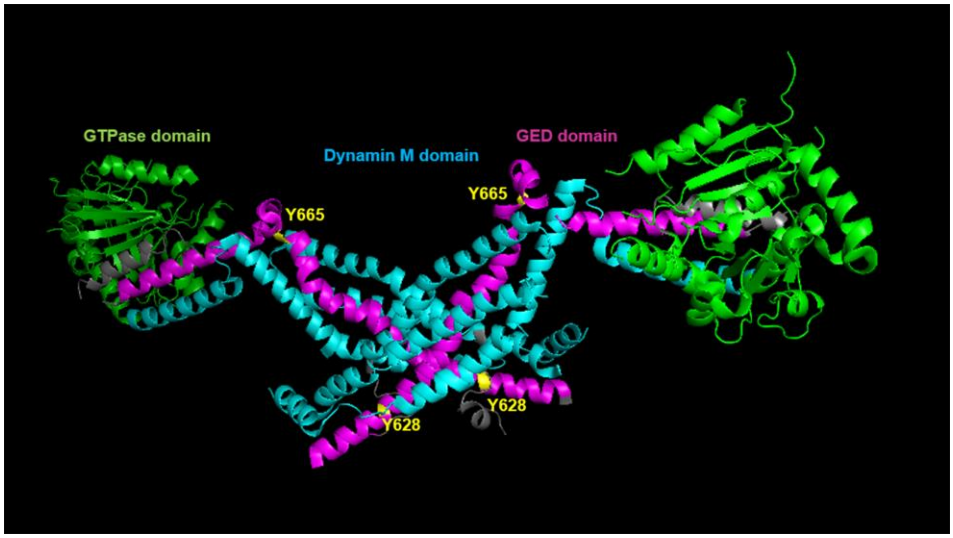

Fig 8. The tyrosine nitration of Drp1 located in GED domain. 3D structure of dimer Drp1. Predicted ribbon structure of human Drp1 showing nitration modification.

3.7. Nitration of Drp1 has no effect GTPase activity but stimulates its aggregation.

We finally investigated the impacts of nitrated modifications on GTPase activity or oligomers/polymers formation of Drp1. We determined the GTPase Drp1 enzymatic activity in the spinal cords of EAE mice (18dpi) and control mice. As showed in Fig. 9A, there was no significant difference in the GTPase activity of the spinal cords between the control mice and the EAE mice (18dpi). We also detected the GTPase activity in human recombinant Drp1 with or without $ONOO^-$ exposure. As expected, the *in vitro* study by using recombinant Drp1 exposed $ONOO^-$ treatment yielded similar results to the *in vivo* EAE animal experiments (Fig. 9B). We then detected oligomerization/polymerization of Drp1. Western blot analysis showed that Drp1 oligomer/polymer levels in the spinal cords were coincident with the clinical scores and disease progression in EAE mice with simultaneous peak time at 18 dpi, which were reversed by PDC treatment (Fig. 9C, D). Similarly, $ONOO^-$ donor induced oligomer/polymer formation of Drp1 in the cultured SH-SY5Y cells, which was also abolished by PDC treatment (Fig. 9E). Since the nitrative modifications of Drp1 induced its aggregation *in vivo,* we speculated whether in the *in vitro* study on the nitration of Drp1 would be similar to the *in vivo* study. Indeed, incubation of recombinant Drp1 protein with synthesized sodium $ONOO^-$ increased the generation of high molecular weight SDS-resistant oligomers/polymers (Fig. 9F). Finally, we confirmed our western blot results by detecting the morphology of Drp1 or nitrated Drp1 using TEM (Fig. 9G). Taken together, those results suggest that $ONOO^-$-mediated Drp1 assembly and mitochondrial recruitment could mediate mitophagy activation and aggravate disease progression in the EAE pathogenesis.

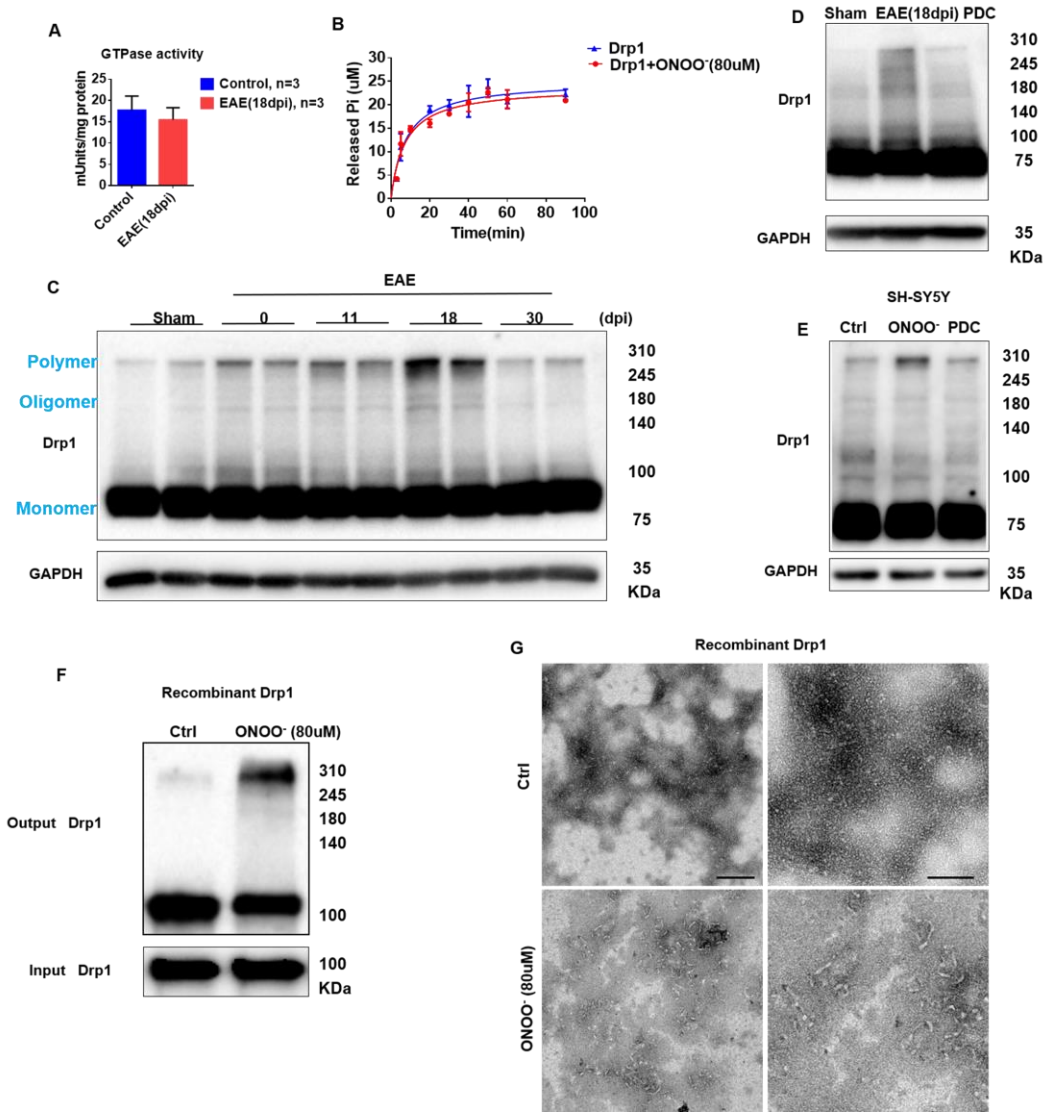

Fig 9. The nitration of Drp1 affected the Drp1 oligomer/polymer formation rather than GTPase activity. (A) GTPase enzymatic activity in spinal cord tissues from vehicle or immunized mice (18dpi). **(B)** GTPase activity of recombinant Drp1(0.5 μM) or $ONOO^-$ (80 μM) -incubated Drp1 plotted as concentration of Pi released over time. **(C)** Western blot detection of monomer/oligomer/polymer Drp1 expressions in spinal cords of active EAE mice at different phases. **(D)** Western blot images of monomer/oligomer/polymer Drp1 expressions in spinal cords of vehicle, active EAE or PDC-treated EAE mice at peak of disease (18dpi). **(E)** Western blot detection of monomer/oligomer/polymer Drp1 expressions in SH-SY5Y cells exposed to vehicle, $ONOO^-$(80 μM) or $ONOO^-$ plus PDC (50 μM). **(F)** Western blot images of human recombinant Drp1(0.5 μM) or $ONOO^-$ -incubated Drp1 protein following Drp1 antibody blotting. **(G)** Electron micrographs of negatively stained recombinant Drp1 in the presence of vehicle or $ONOO^-$ (80 μM) for 30 min. Scale bar, 100 nm and 50 nm corresponding 2× zoom of regions of interest.

4. Discussion

Autophagy appears to have dual neuroprotective and detrimental roles in MS/EAE pathology, relying on its levels, involved cell-types, inflammatory/ autoimmune status and disease progress stages. Neurons are inflammatory/ autoimmune target cells and ultimately damaged during MS/EAE pathology, resulting in paresis or paralysis. The roles of neuronal autophagy in MS pathology and its underlying mechanisms remain unclear yet. Herewith, we investigated the dynamic changes of autophagy at different stages of EAE *in vivo* and found that autophagy activation was coincidently increased with axonal damage, apoptosis and disease progression in the CNS lesions of active EAE mice. Autophagy activation was mainly orientated in neurons and reached its maximum at peak time of disease (18 dpi). Treatment of 3-MA, an autophagy inhibitor, alleviated EAE neurological defect throughout the disease course. Those results suggest that excessive neuronal autophagy might contribute to the CNS damages and the disease progression in EAE pathology.

Mitochondria dysfunction, the earliest hallmark of MS, is a prerequisite for axon damage and neuronal injury. Mitochondrial damage was found in CNS motor neurons from MS patients [43-45]. Mitophagy is highly activated in CNS lesion of the EAE mice and the patients died from MS [46, 47]. Mitochondrial recruitment of Drp1 is essential step for mitophagy fission/fragmentation, and PINK1/Parkin pathway subsequently regulates the mitophagic process to degrade damaged mitochondria [36, 37]. Inhibition of Drp1 translocation to the mitochondria reduced mitochondrial fragmentation, the loss of oligodendrocytes and demyelination in EAE model [22]. Mitochondrial division/mitophagy inhibitor Mdivi-1 blocked the phosphorylation of Drp1, inhibited mitochondrial fragmentation and attenuated kainic acid induced neuronal cell death [48]. In the present study, we found that Drp1 mitochondrial recruitment was a crucial step in the PINK1/Parkin-mediated mitophagy, which was predominant in the neurons of the spinal cords in active EAE mice. Mdivi-1 treatment

remarkably suppressed the mitochondrial translocation of Drp1, inhibited PINK1/Parkin-mediated mitophagy, alleviated EAE symptoms, postponed disease progression and reduced the disease severity. Those results provide a clue that Drp1 translocation to mitochondria could be a critical step for neuronal mitophagy activation during EAE pathogenesis.

Mitochondria are the direct targets of $ONOO^-$ to induce mitochondria dysfunction during MS/EAE pathogenesis [26, 49]. Our recent study revealed that PDC treatment inhibited the recruitment of Drp1 into the damaged mitochondria and suppressed mitophagy activation in experimental ischemic stroke model [25]. However, the roles of $ONOO^-$ in Drp1 mitochondrial translocation and mitophagy activation in EAE pathology are unknown. ROS/RNS, derived from activated macrophages/ microglia, can trigger mitochondrial pathology [14]. As a representative RNS, $ONOO^-$ has strongly membrane penetrability and highly cytotoxicity to CNS, inducing axonal degeneration and neuronal cell death during EAE/MS [50]. Increased 3-NT was found in serum, CSF and CNS of the MS patients as well as EAE mice [51, 52]. Thus, we explored the underlying mechanisms of $ONOO^-$ in activating neuronal mitophagy during EAE pathology. By using our newly developed fluorescent probes, we found the elevated $ONOO^-$ level in the serum and the spinal cords of the EAE mice, consistent with the results of 3-NT. Importantly, the increased $ONOO^-$ production was coincident with axonal damages, clinical scores and disease progression. The levels of $ONOO^-$ in the serum and the spinal cords reached to the peak at 18 dpi, matched well with the activated autophagy and the disease severity in the active EAE mice. Furthermore, the co-localization of MitoPN-1 fluorescence with MAP-2 revealed the elevated mitochondrial $ONOO^-$ production specifically in the neurons of the spinal cords during EAE pathogenesis (18dpi). Given that increased $ONOO^-$ level was consistent with activated autophagy/mitophagy and EAE neurological damages, we proposed that $ONOO^-$ could be sufficient to induce mitophagy activation. In supporting this assumption, PDC treatment reduced $ONOO^-$ level, suppressed PINK1/Parkin-mediated mitophagy activation and the mitochondrial recruitment of Drp1 in the neurons, and attenuated the neurological defect scores in the active EAE

mice. Consistently, in the cultured SH-SY5Y cells and primary neurons, the treatment of exogenous synthesized $ONOO^-$ remarkably activated Drp1-mediated mitophagy and triggered apoptotic cell death, which were abolished by PDC treatment. In addition, to better mimic *in vivo* situations, we also employed SIN-1 as an endogenous $ONOO^-$ donor to produce $O_2^{\bullet-}$ and NO simultaneously, rapidly forming $ONOO^-$ in biological systems. In line with the results of synthesized sodium $ONOO^-$ experiments, SIN-1 treatment induced mitophagy activation in SH-SY5Y with Drp1 mitochondrial accumulation, which were reversed by PDC intervention, implying $ONOO^-$ could be sufficient to trigger mitophagy activation (Supplementary Fig. 4). Together, these results suggest that $ONOO^-$ could be a crucial player in PINK1/Parkin-mediated mitophagy activation via triggering mitochondrial recruitment of Drp1, leading to neurological injury during EAE pathology.

As an initial step of mitophagy, mitochondrial fission is a stepwise reaction regulated by Drp1 recruitment, oligomerization, polymer assembly, subsequently mitochondrial membrane constriction and GTP hydrolysis. Thus, we investigated the effects of $ONOO^-$ on Drp1 during EAE injury. We found that $ONOO^-$ recruited Drp1 to the damaged mitochondria and then activated mitophagy in the spinal cords of active EAE mice. The *in vitro* cell experiments yielded the similar results when the cells were treated by synthesized sodium $ONOO^-$ or SIN-1. Those results suggest that $ONOO^-$ could mediate the recruitment of Drp1 into mitochondria for activating mitophagy.

Next, we logically addressed whether and how $ONOO^-$ affects the functions of Drp1 and leads the Drp1 mitochondrial recruitment for mitophagy activation. Posttranslational modification implicates in the regulation of Drp1 function under diverse cellular stimuli, including phosphorylation, S-nitrosylation, ubiquitination, and SUMOylation. Emerging evidence indicate that Drp1 is comparatively vulnerable to nitrosative and nitrative stress [23, 25, 53]. NO could trigger mitochondrial fission and neuronal injury *via S*-nitrosylation of Drp1 [21]. The precise impacts of Drp1 nitration on its functions and mitophagy activation in EAE pathology remain obscure. Thus, we investigated the nitration of Drp1 in CNS of active EAE mice. Two tyrosine

nitration of Drp1 peptides LIKSYFLIVR (Y 628) and AVMHFLVNHVKDTLQSELVGQLYK (Y 665) were found to locate at GED domain, which could mediate GTPase activity or/and Drp1 oligomers/polymers formation. More excitingly, we found that $ONOO^-$ induced Drp1 oligomerization/ polymerization *in vivo* rather than GTPase activity. Notably, there are two major challenges in data interpretations. The first challenge is to distinguish the nitrated proteins acting as causal drivers of the pathology from collateral damage; the second is that other free radicals in biological systems might also participate in the oxidation of Drp1. To solve these problems, we designed the *in vitro* experiments by exploring recombinant human Drp1 protein to $ONOO^-$ directly and examined the impacts of $ONOO^-$ on Drp1 function. As expected, the *in vitro* results were consistent with the *in vivo* EAE animal model. Subsequently, targeting nitrated Drp1 could be a novel therapeutic approach for MS. Nevertheless, we should note that other amino acids, such as cysteine and tryptophan, could be also the targets for oxidation and regulate Drp1 functions [54]. Still, further study is needed to exclude other potential modification influences and elucidate the exact effects of tyrosine nitration on Drp1 mitochondrial division.

In conclusion, we demonstrate that the critical involvement of $ONOO^-$-mediated excessive mitophagy in EAE/MS pathogenesis. To our knowledge, this is a first report that $ONOO^-$ could trigger PINK1/Parkin-mediated mitophagy activation via inducing Drp1 nitration modification and assembly, leading to neurological deficits in EAE pathogenesis. The $ONOO^-$ -mediated Drp1 assembly and mitochondrial recruitment could be a critical pathological process with the potentials for developing novel therapeutic approaches for MS.

Study approval

All animal experiments were approved by the Committee on the Use of Live Animals in Teaching and Research at the University of Hong Kong.

Acknowledgements

This study is supported Research Grants Council AoE/P-705/16 grant and RGC

GRF grant (No. 17118514), Hong Kong. We thank Faculty Core Facility, Li Ka Shing Faculty of Medicine, the University of Hong Kong to supply Carl Zeiss LSM 780/800, dSTORM for capturing confocal fluorescent images, Electron Microscope Unit for TEM assistance and Proteomics & Metabolomics Core Facility for assistance in LC-MS/MS.

Author contributions

WT-L performed most of the experiments, analyzed the data and wrote the manuscript. JH-F helped to conduct autophagy/mitophagy analysis, GC assisted in capturing images, ML-W offered assistant for LC-MS/MS data searching, QH-D contributed to Drp1 3D structure drawing and BT helped for primary neuron culture handling. DY developed and supplied the $ONOO^-$ detection probes, including HKyellow, HKyellow-AM and MitoPN-1. QW contributed to EAE animal experiments, data interpretation and manuscript preparation, JG-S designed and supervised the whole research activities, revised the manuscript and obtained the funding for the study. All authors have read and agreed with the manuscript.

Conflict of interest

All authors have declared no competing financial interests.

References

1. Thompson, A.J., A.T. Toosy, and O. Ciccarelli, Pharmacological management of symptoms in multiple sclerosis: current approaches and future directions. Lancet Neurol., 2010. **9**(12): p. 1182-1199.
2. Lassmann, H. and J. van Horssen, The molecular basis of neurodegeneration in multiple sclerosis. FEBS Lett., 2011. **585**(23): p. 3715-23.
3. Mizushima, N. and M. Komatsu, Autophagy: renovation of cells and tissues. Cell, 2011. **147**(4): p. 728-41.
4. Hara, T., et al., Suppression of basal autophagy in neural cells causes neurodegenerative disease in mice. Nature, 2006. **441**(7095): p. 885-9.
5. Chung, Y., et al., Dysregulated autophagy contributes to caspase-dependent neuronal apoptosis. Cell Death Dis, 2018. **9**(12): p. 1189.
6. Liang, P. and W. Le, Role of autophagy in the pathogenesis of multiple sclerosis. Neurosci Bull, 2015. **31**(4): p. 435-44.
7. Kovacs, J.R., et al., Autophagy promotes T-cell survival through degradation of proteins of the cell death machinery. Cell Death Differ, 2012. **19**(1): p. 144-52.
8. Bhattacharya, A., et al., Deficiency of autophagy in dendritic cells protects against experimental autoimmune encephalomyelitis. J Biol Chem, 2014. **289**(38): p. 26525-32.
9. Bhattacharya, A., et al., Autophagy Is Required for Neutrophil-Mediated Inflammation. Cell Rep, 2015. **12**(11): p. 1731-9.
10. Campbell, G.R., J.T. Worrall, and D.J. Mahad, The central role of mitochondria in axonal degeneration in multiple sclerosis. Mult Scler, 2014. **20**(14): p. 1806-13.
11. Witte, M.E., et al., Reduced expression of PGC-1alpha partly underlies mitochondrial changes and correlates with neuronal loss in multiple sclerosis cortex. Acta Neuropathol, 2013. **125**(2): p. 231-43.
12. Patergnani, S., et al., Mitochondria in Multiple Sclerosis: Molecular Mechanisms of Pathogenesis. Int Rev Cell Mol Biol, 2017. **328**: p. 49-103.
13. Kamat, P.K., et al., Autophagy of mitochondria: a promising therapeutic target for neurodegenerative disease. Cell Biochem Biophys, 2014. **70**(2): p. 707-19.
14. Nikic, I., et al., A reversible form of axon damage in experimental autoimmune encephalomyelitis and multiple sclerosis. Nat. Med., 2011. **17**(4): p. 495-9.
15. Bishop, A., et al., Differential sensitivity of oligodendrocytes and motor neurons to reactive nitrogen species: implications for multiple sclerosis. J Neurochem, 2009. **109**(1): p. 93-104.
16. Dujmovic, I., et al., Cerebrospinal fluid and serum uric acid levels in patients with multiple sclerosis. Clin Chem Lab Med, 2009. **47**(7): p. 848-53.
17. Guerrero, A.L., et al., Variation of serum uric acid levels in multiple sclerosis during relapses and immunomodulatory treatment. Eur J Neurol, 2008. **15**(4): p. 394-7.
18. Bolton, C., et al., The acute and chronic phases of chronic relapsing experimental autoimmune encephalomyelitis (CR EAE) are ameliorated by the peroxynitrite decomposition catalyst, 5,10,15,20-tetrakis(4-sulfonatophenyl)porphyrinatoiron (III) chloride, (FeTPPS). Eur J Pharmacol, 2008. **601**(1-3): p. 88-93.
19. Vana, A.C., et al., Arachidonyl trifluoromethyl ketone ameliorates experimental autoimmune encephalomyelitis via blocking peroxynitrite formation in mouse spinal cord white matter.

Exp Neurol, 2011. **231**(1): p. 45-55.
20. Buhlman, L., et al., Functional interplay between Parkin and Drp1 in mitochondrial fission and clearance. Biochim Biophys Acta, 2014. **1843**(9): p. 2012-26.
21. Cho, D.H., et al., S-nitrosylation of Drp1 mediates beta-amyloid-related mitochondrial fission and neuronal injury. Science, 2009. **324**(5923): p. 102-5.
22. Luo, F., et al., Inhibition of Drp1 hyper-activation is protective in animal models of experimental multiple sclerosis. Exp Neurol, 2017. **292**: p. 21-34.
23. Nakamura, T., et al., S-nitrosylation of Drp1 links excessive mitochondrial fission to neuronal injury in neurodegeneration. Mitochondrion, 2010. **10**(5): p. 573-8.
24. Qi, X., et al., Mitochondrial protein nitration primes neurodegeneration in experimental autoimmune encephalomyelitis. J Biol Chem, 2006. **281**(42): p. 31950-62.
25. Feng, J., et al., Inhibition of Peroxynitrite-Induced Mitophagy Activation Attenuates Cerebral Ischemia-Reperfusion Injury. Mol Neurobiol, 2018. **55**(8): p. 6369-6386.
26. Li, W., et al., Radix Rehmanniae Extract Ameliorates Experimental Autoimmune Encephalomyelitis by Suppressing Macrophage-Derived Nitrative Damage. Front Physiol, 2018. **9**: p. 864.
27. Chen, X., et al., Peroxynitrite enhances self-renewal, proliferation and neuronal differentiation of neural stem/progenitor cells through activating HIF-1alpha and Wnt/beta-catenin signaling pathway. Free Radic Biol Med, 2018. **117**: p. 158-167.
28. Yu, J., et al., Genetic ablation of dynactin p150(Glued) in postnatal neurons causes preferential degeneration of spinal motor neurons in aged mice. Mol Neurodegener, 2018. **13**(1): p. 10.
29. Gong, J., et al., Momordica charantia polysaccharides could protect against cerebral ischemia/reperfusion injury through inhibiting oxidative stress mediated c-Jun N-terminal kinase 3 signaling pathway. Neuropharmacology, 2015. **91**: p. 123-34.
30. Peng, T., et al., A rationally designed rhodamine-based fluorescent probe for molecular imaging of peroxynitrite in live cells and tissues. Chem Sci, 2016. **7**(8): p. 5407-5413.
31. Yang, D., et al., A highly selective fluorescent probe for the detection and imaging of peroxynitrite in living cells. J Am Chem Soc, 2006. **128**(18): p. 6004-5.
32. Manczak, M. and P.H. Reddy, Abnormal interaction between the mitochondrial fission protein Drp1 and hyperphosphorylated tau in Alzheimer's disease neurons: implications for mitochondrial dysfunction and neuronal damage. Hum Mol Genet, 2012. **21**(11): p. 2538-47.
33. Shirendeb, U.P., et al., Mutant huntingtin's interaction with mitochondrial protein Drp1 impairs mitochondrial biogenesis and causes defective axonal transport and synaptic degeneration in Huntington's disease. Hum Mol Genet, 2012. **21**(2): p. 406-20.
34. Yan, J., et al., Blockage of GSK3beta-mediated Drp1 phosphorylation provides neuroprotection in neuronal and mouse models of Alzheimer's disease. Neurobiol Aging, 2015. **36**(1): p. 211-27.
35. Shi, R., et al., Excessive autophagy contributes to neuron death in cerebral ischemia. CNS Neurosci Ther, 2012. **18**(3): p. 250-60.
36. Otera, H., N. Ishihara, and K. Mihara, New insights into the function and regulation of mitochondrial fission. Biochim Biophys Acta, 2013. **1833**(5): p. 1256-68.
37. Sebastian, D., M. Palacin, and A. Zorzano, Mitochondrial Dynamics: Coupling Mitochondrial Fitness with Healthy Aging. Trends Mol Med, 2017. **23**(3): p. 201-215.

38. Zhu, P.P., et al., Intra- and intermolecular domain interactions of the C-terminal GTPase effector domain of the multimeric dynamin-like GTPase Drp1. J Biol Chem, 2004. **279**(34): p. 35967-74.
39. Hinshaw, J.E., Dynamin and its role in membrane fission. Annu Rev Cell Dev Biol, 2000. **16**: p. 483-519.
40. Praefcke, G.J. and H.T. McMahon, The dynamin superfamily: universal membrane tubulation and fission molecules? Nat Rev Mol Cell Biol, 2004. **5**(2): p. 133-47.
41. van der Bliek, A.M., Functional diversity in the dynamin family. Trends Cell Biol, 1999. **9**(3): p. 96-102.
42. Nishida, K., et al., Dynamic recruitment of dynamin for final mitochondrial severance in a primitive red alga. Proc Natl Acad Sci U S A, 2003. **100**(4): p. 2146-51.
43. Ashrafi, G. and T.L. Schwarz, The pathways of mitophagy for quality control and clearance of mitochondria. Cell Death Differ, 2013. **20**(1): p. 31-42.
44. Mahad, D., et al., Mitochondrial defects in acute multiple sclerosis lesions. Brain, 2008. **131**(Pt 7): p. 1722-35.
45. Mahad, D.J., et al., Mitochondrial changes within axons in multiple sclerosis. Brain, 2009. **132**(Pt 5): p. 1161-74.
46. Broadwater, L., et al., Analysis of the mitochondrial proteome in multiple sclerosis cortex. Biochim Biophys Acta, 2011. **1812**(5): p. 630-41.
47. Patergnani, S., et al., Autophagy and mitophagy elements are increased in body fluids of multiple sclerosis-affected individuals. J Neurol Neurosurg Psychiatry, 2017.
48. Kim, H., et al., A mitochondrial division inhibitor, Mdivi-1, inhibits mitochondrial fragmentation and attenuates kainic acid-induced hippocampal cell death. BMC Neurosci, 2016. **17**(1): p. 33.
49. Vattemi, G., et al., Increased protein nitration in mitochondrial diseases: evidence for vessel wall involvement. Mol Cell Proteomics, 2011. **10**(4): p. M110 002964.
50. Dunham, J., et al., Oxidative Injury and Iron Redistribution Are Pathological Hallmarks of Marmoset Experimental Autoimmune Encephalomyelitis. J. Neuropathol. Exp. Neurol., 2017. **76**(6): p. 467-478.
51. Bolton, C., et al., The acute and chronic phases of chronic relapsing experimental autoimmune encephalomyelitis (CR EAE) are ameliorated by the peroxynitrite decomposition catalyst, 5,10,15,20-tetrakis(4-sulfonatophenyl)porphyrinatoiron (III) chloride, (FeTPPS). Eur. J. Pharmacol., 2008. **601**(1-3): p. 88-93.
52. Jack, C., et al., Contrasting potential of nitric oxide and peroxynitrite to mediate oligodendrocyte injury in multiple sclerosis. Glia, 2007. **55**(9): p. 926-34.
53. Lee, D.S. and J.E. Kim, PDI-mediated S-nitrosylation of DRP1 facilitates DRP1-S616 phosphorylation and mitochondrial fission in CA1 neurons. Cell Death Dis, 2018. **9**(9): p. 869.
54. Thompson, S., et al., Regulation of Chemokine Function: The Roles of GAG-Binding and Post-Translational Nitration. Int J Mol Sci, 2017. **18**(8).

Supplementary materials

Materials and methods

Nitrotyrosine (NT) level detection

To detect the dynamic levels of nitrotyrosine (NT) in serum during EAE pathogenesis, the serum of EAE mice at different time points (0, 5, 10, 15, 20, 25 and 30dpi) were collected respectively. In detail, serum was prepared followed by centrifuged at 1000g for 15 min and was stored at − 80 °C for enzyme-linked immunosorbent assay (ELISA) analysis. Serum NT level was determined with a commercially available ELISA kit from USCN (Wuhan, China).

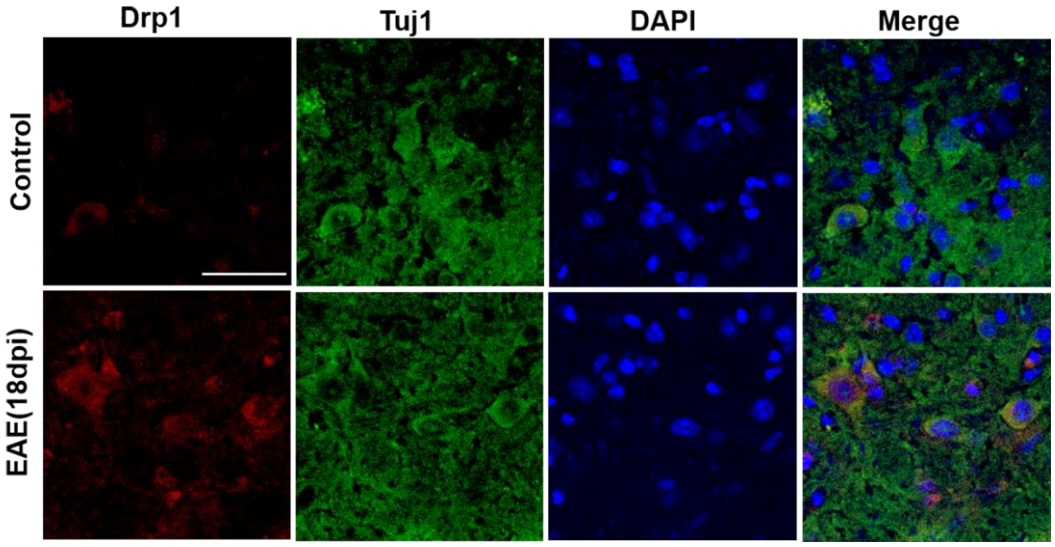

Supplementary Fig 1. The redistribution of Drp1 occurred in neurons of the EAE-induced spinal cords. Co-immunostaining images of Drp1 (red), neuronal marker TuJ1 (Green), and nuclear (blue) in control and active EAE groups (18dpi). Scale bar, 50 μm. (n = 3 mice/group).

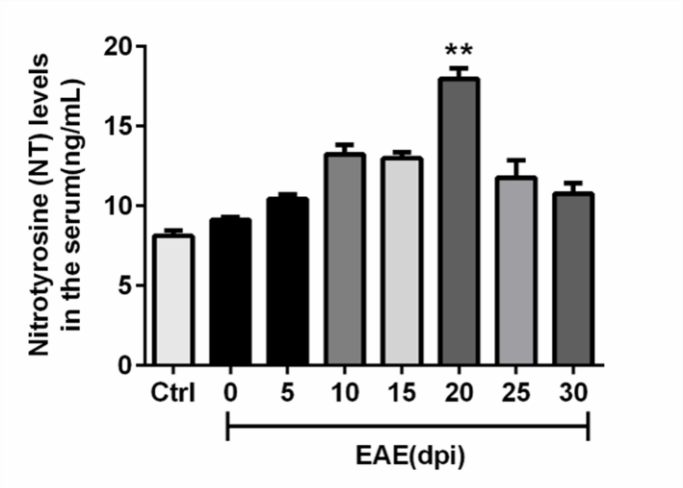

Supplementary Fig 2. Nitrotyrosine productions were largely generated in the serum of active EAE mice, coinciding with EAE progression. Serum NT levels detection in time-dependent active EAE mice after active immunization by ELISA assay. (n = 3 mice/group, **P < 0.01, versus the control group (one-way ANOVA followed by Dunnett's multiple-comparison test).

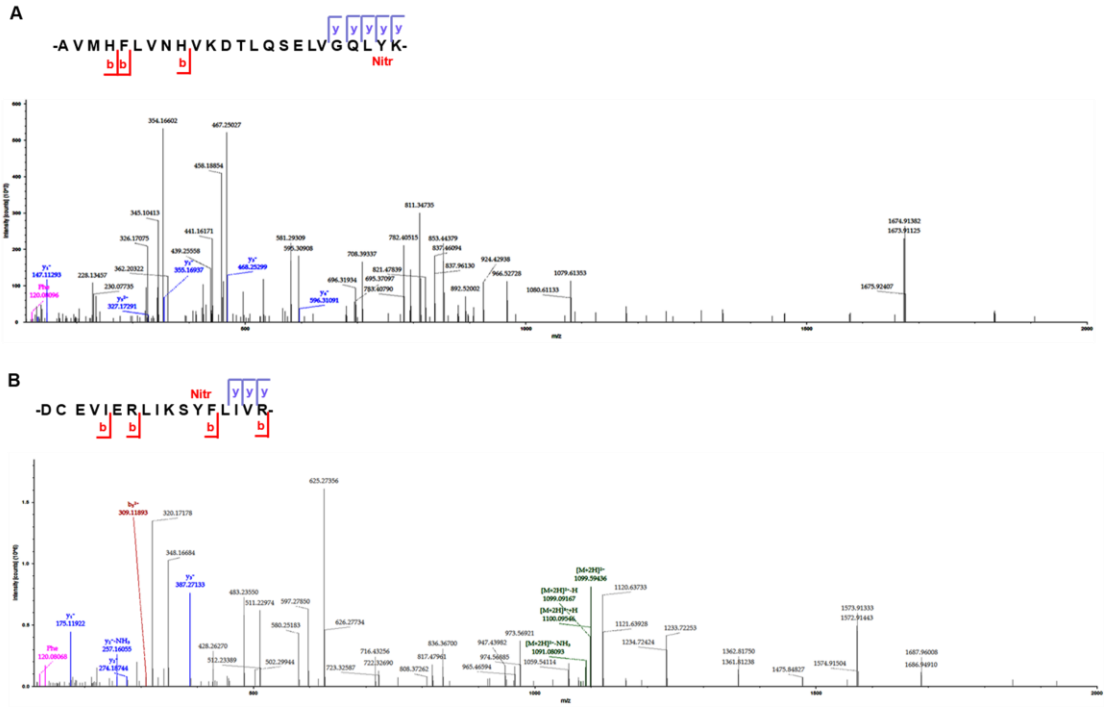

Supplementary Fig 3. Mass spectrogram of Drp1 peptide sequences contained with tyrosine nitration residues in the spinal cords of active EAE mice (18dpi).

(A) Mass spectrogram of AVMHFLVNHVKDTLQSELVGQLYK with nitrated Y665

(B) Mass spectrogram of DCEVIERLIKSYFLIVR with nitrated Y628.

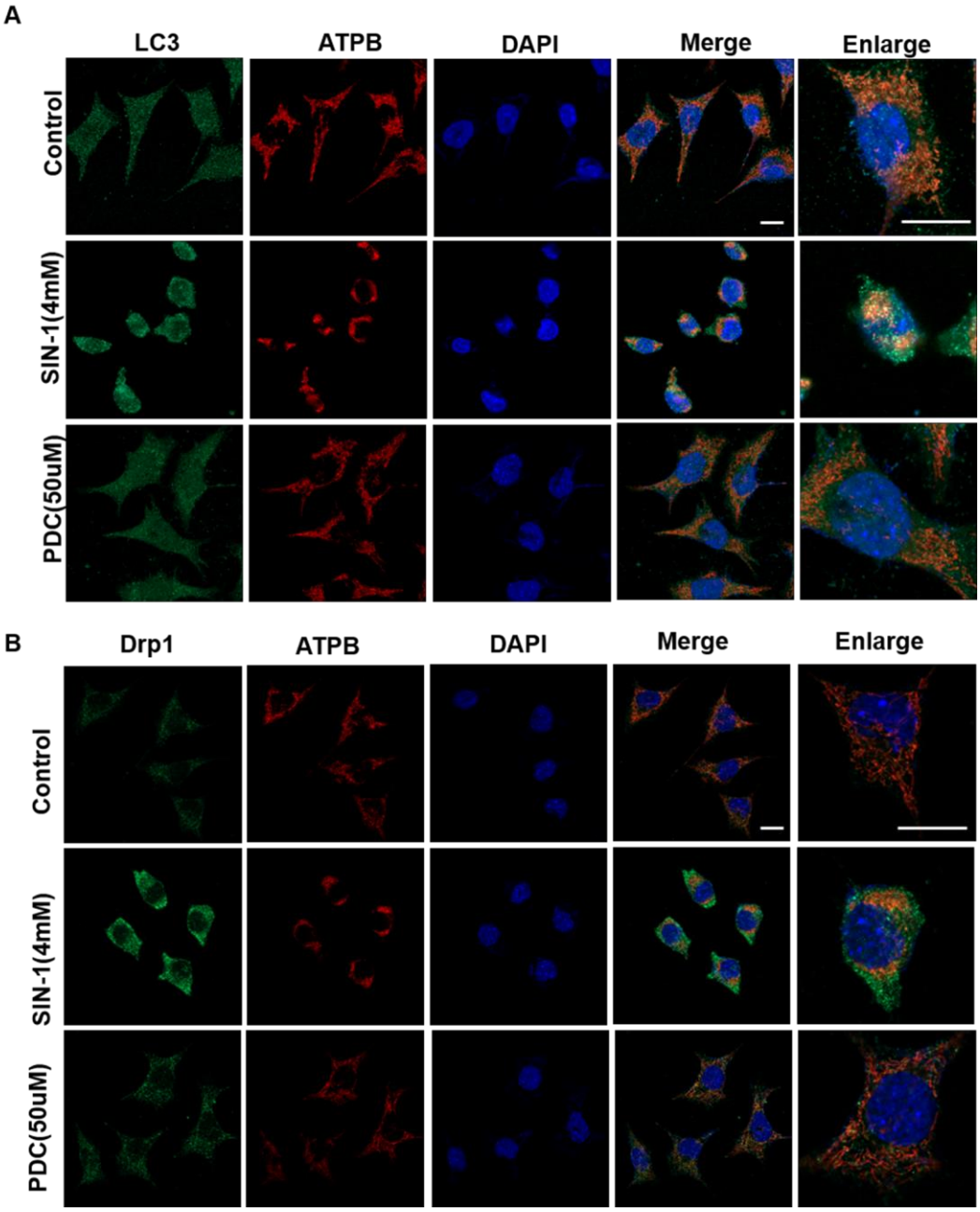

Supplementary Fig 4. PDC inhibited mitophagy activation with suppressing Drp1 mitochondrial recruitment in SH-SY5Y cells exposed to peroxynitrite. SH-SY5Y cells were exposed to a $ONOO^-$ donor SIN-1 for 2h to induce nitrative stress. Immunofluorescent co-staining of LC3 with ATPB **(A)** and Drp1 with ATPB **(B)** in SH-SY5Y cells of control, SIN-1(4mM) and PDC-treated groups (50 μM). Scale bars, 5 μm.

Supplementary Table 1. Primary antibodies used in this study.

Antibodies	Source	Catology No.	Dilution		
			WB	IF	IP
Amyloid precursor protein (APP)	Abcam	ab32136	1:1000	-	-
MAP-2	Cell Signaling Technology	8707	-	1:400	-
Choline Acetyltransferase (ChAT)	Millipore	AB144P	-	1:200	-
HSP60	Abcam	ab46798	-	1:400	-
Bcl-2	Cell Signaling Technology	2876	1:1000	-	-
Bax	Cell Signaling Technology	2772	1:1000	-	-
LC3	Abcam	ab128025	1:1000	1:400	-
Parkin	Abcam	ab15954	1:1000		-
Drp1	Cell Signaling Technology	14647	1:1000	1:400	-
Drp1	Cell Signaling Technology	8570	-	-	1:100
PINK1	Abcam	ab63950	1:1000	-	-
iNOS	Abcam	ab3523	1:1000		-
p47^{phox}	Santa Cruz	sc-7660	1:500	-	-
P67^{phox}	Santa Cruz	sc-374510	1:500	-	-
3-Nitrotyrosine (3-NT)	Abcam	ab61392	1:1000	1:50	-
β-Tubulin III (Tuj-1)	Covance	MMS-435P	-	1:400	-
GAPDH	Merck Millipore	AB2302	1:1000	-	-
ATPB	Abcam	ab14730	1:1000	1:400	-
VDAC1/Porin	Abcam	ab15895	1:1000	-	-

Western blot, WB; Immunofluorescence, IF; Immunoprecipitation, IP.